NTNU – Trondheim
Norwegian University of
Science and Technology

Closed Mould Net Shape Processing of Prepregs with Resin Injection

Simen Johnsen

Master of Science in Mechanical Engineering
Submission date: June 2013
Supervisor: Andreas Echtermeyer, IPM

Norwegian University of Science and Technology
Department of Engineering Design and Materials

THE NORWEGIAN UNIVERSITY
OF SCIENCE AND TECHNOLOGY
DEPARTMENT OF ENGINEERING DESIGN
AND MATERIALS

MASTER THESIS SPRING 2013
FOR
STUD.TECHN. SIMEN JOHNSEN

Closed Mould Net Shape Processing of Prepregs with Resin Injection

High quality composite parts need to have well controlled fiber placement and matrix content. The shape of the produced part shall fit into tight tolerances without any further machining after production. SQRTM is a semi-automated process that can be used for making such parts.

This project shall explore how void content and surface roughness can be controlled. The effect of flow patterns and surface layers shall be investigated. Process parameters shall be varied and controlled.

The thesis should include the signed problem text, and be written as a research report with summary both in English and Norwegian, conclusion, literature references, table of contents, etc. During preparation of the text, the candidate should make efforts to create a well arranged and well written report. To ease the evaluation of the thesis, it is important to cross-reference text, tables and figures. For evaluation of the work a thorough discussion of results is appreciated. Safety evaluations for experimental work shall be added to the Appendix.

Three weeks after start of the thesis work, an A3 sheet illustrating the work is to be handed in. A template for this presentation is available on the IPM's web site under the menu "Masteroppgave" (http://www.ntnu.no/ipm/masteroppgave). This sheet should be updated one week before the Master's thesis is submitted.

The thesis shall be submitted electronically via DAIM, NTNU's system for Digital Archiving and Submission of Master's thesis.

Torgeir Welo
Head of Division

Andreas Echtermeyer
Professor/Supervisor

NTNU
Norges teknisk-
naturvitenskapelige universitet
Institutt for produktutvikling
og materialer

Norges teknisk-naturvitenskapelige universitet

Sammendrag

Fakultet for ingeniørvitenskap og teknologi
Institutt for produktutvikling og materialer

Mastergrad i teknologi

Fremstilling av kompositttdeler i lukkede hulrom med resininjeksjon

ved Simen Johnsen

Avanserte kompositttdeler krever strenge toleranser i alle retninger før delene er klare til å brukes. Mange maskinerings- og sammenstillingsoperasjoner er ofte nødvendig for å oppnå ønsket geometri og toleranser. Nye metoder for å fremstille avansert geometri og strenge toleranser er ønskelig for å minimere antall operasjoner.

En ny lukket form- metode som utnytter karbonfiber prepreg-materialer i tillegg til injeksjon av resin har blitt testet og evaluert. En rigg som implementerer denne lukket form- teknikken ble bygget og brukt til å produsere generiske deler. I tillegg har numeriske analyser blitt utført for å forstå resultatene av testene. Delene som fremkom ble også utsatt for en trepunkts bøyeprøve. Karbonfiberdeler uten overflatefeil og indre feil ble oppnådd når de riktige forholdsregler ble tatt. Den lukkede form teknikken som presenteres i denne avhandlingen vil i stor grad redusere antallet arbeidsoperasjoner som er nødvendige for å produsere avanserte kompositttdeler. Ved resin-injeksjon og korrekt håndtering av materialene før støping kan høykvalitets deler oppnås.

NORWEGIAN UNIVERSITY OF SCIENCE AND TECHNOLOGY

Abstract

Faculty of Engineering Science and Technology
Department of Engineering Design and Materials

Master of Science

Closed Mould Net Shape Processing of Prepregs with Resin Injection

by Simen Johnsen

High performance composite parts require strict tolerances in all directions before the parts are ready to be used. Numerous of machining and assembly operations are often required to obtain the desired geometry and tolerances. New methods to acquire advanced geometry and tight tolerances are desired to minimize the numbers of assembly and machining operations.

A new closed mould technique utilizing carbon fibre prepreg materials and resin injection has been tested and evaluated. A rig implementing the closed mould technique was built and used to produce generic parts. Additionally numerical analyses were run in order to understand results of the tests. The parts obtained were also subjected to a three point bending test. High quality carbon fibre parts without surface flaws or internal voids were achieved when the right precautions were taken. The closed mould technique presented in this thesis will greatly minimize the numbers of machining operations necessary to obtain a high performance composite part. By resin injection and correct pre mould handling of the materials high quality parts are obtained.

Preface

This thesis consists of 12 chapters and 5 appendices. It is written as my master's thesis at the *Institute of Engineering Design and Materials* at *The Norwegian University of Science and Technology*. I have previously conducted a project work as a pre study for this thesis, named *Closed Form Net Shape Processing of Composites*. This report is written in cooperation with Kongsberg Defense Systems. The work is in its entirety conducted by me. I would like to express my deepest gratitude to my supervisors: Professor Andreas Echtermyer at NTNU and Tor Sigurd Breivik at KDA for giving me the opportunity to work with this interesting technology and providing excellent support throughout the process. I would also like to thank Alf Pettersen at KDA for providing funding, both for the project and trips to KDA for guiding and knowledge transfer. Further thanks are expressed to Nils Petter Vedvik, Børge Holen, Halvard Støwer and Bjarne Stolpnessæter for help and advice with computer simulations, and production of the setup.

Trondheim June 10, 2013

Simen Johnsen

Contents

List of Figures

List of Tables

Abbreviations

SQRTM	**S**ame **Q**ualified **R**esin **T**ransfer **M**oulding
RTM	**R**esin **T**ransfer **M**oulding
CFRP	**C**arbon **F**ibre **R**einforced **P**olymer
FEA	**F**inite **E**lement **A**nalysis
LSM	**L**aminate **S**tiffness **M**atrix
CFD	**C**omputational **F**luid **D**ynamics
OOA	**O**ut **O**f **A**utoclave processing
LCM	**L**iquid **C**omposite **M**oulding
UD	**U**ni **D**irectional
CTE	**C**oefficient of **T**hermal **E**xpansion
WCS	**W**ork **C**oordinate **S**ystem
v_f	Fibre volume fraction
S11	Normal stress in material orientation 1
S33	Normal stress in material orientation 3
X_T	Ultimate tensile strength in X-direction
X_C	Ultimate compression strength in X-direction

Chapter 1

Introduction

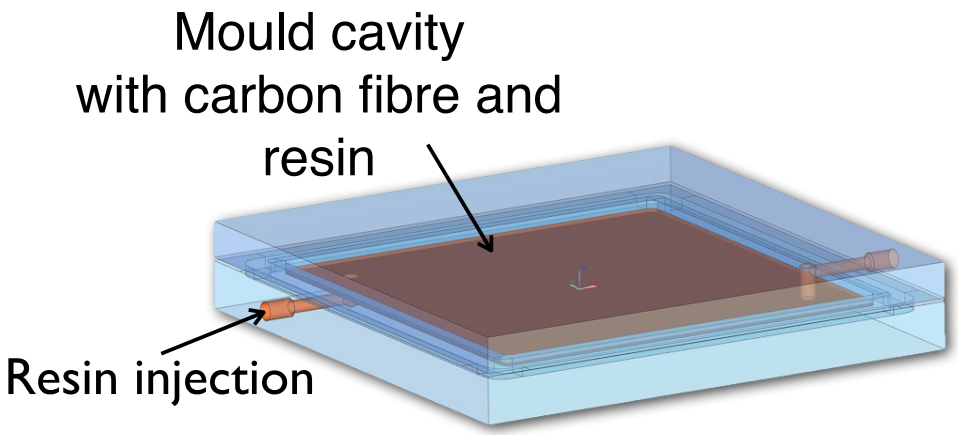

FIGURE 1.1: The picture illustrates the principle of SQRTM with a closed mould where resin is injected through a sprue. The mould cavity is filled with the prepreg preform.

This report is about a method for carbon fibre part production called *Same Qualified Resin Transfer Moulding*, abbreviated *SQRTM* from this point on. SQRTM is an evolution of the much used *Resin Trenasfer Moulding*-process (*RTM*). RTM is thoroughly described by Kruckenberg and Paton [1] and is a technique where a preform of dry fibre reinforcement is placed inside a closed mould tooling and resin is injected to impregnate the preform. The main benefits with this is that

part dimensions can be accurately predicted as the mould surface encloses the part. Hence, post cure machining is kept to a minimum. Research regarding RTM has been carried out in a great extent [2–5]. SQRTM does the same for prepreg as RTM does for dry fibre. It is a closed mould prepreg moulding technique that provides the ability to control resin pressure directly. An explanatory illustration is added in Figure 1.1.

The main objective of this work is to understand the SQRTM process and how it works. Because the technique is merely not documented in the literature whatsoever tests and experiments will be conducted. A closed mould tooling, similar to the one in Figure 1.1, will be used to execute the process. The test samples produced will be tested in three point bending. Additionally numerical simulations will be conducted in order to increase the understanding of the mechanisms involved. The fact that closed mould prepreg consolidation is rare in the literature[1] indicates that it is hard to achieve. Especially ventilation of entrapped air and precipitated volatiles is a challenge that quickly comes to mind.

Prepreg materials consist of fibres and resin. The fibres occupy between 50 % and 64 % of the material volume and the resin ideally inhabit the rest. Prepreg is fabric pre impregnated with resin. The fabric can be woven, stitched or braided in different configurations and patterns. The amount of resin applied is most commonly the amount that is needed for the laminate to be structurally sound. Meaning, there is no excessive resin in the material. The resin is lightly cured, upon application, before the whole material (resin and fabric) is frozen down to prevent further curing of the resin. The material is kept in a frozen state as long as possible until ply collation. There are two main mechanisms that have to be achieved in order to obtain a good laminate. It has to be cured to make it hard and it has to be compacted through the curing process to obtain the desired fibre volume fraction.

In the work with this thesis both contributions from prepreg curing theory and RTM theory have been appreciated.

[1] A search for *Closed OR matched mould prepreg OR pre-preg* on www.scopus.com provides 23 different articles

Chapter 2

Objective

The objective of this thesis can be summarized as follows:

- Understand the SQRTM process and what process parameters that are beneficial.
- Develop CFD models that describe the wet preform flow and pressure propagation.
- Understand the governing mechanisms in the SQRTM process and describe these in a clear and indisputable way.
- Execute physical experiments with the SQRTM technology and produce simple parts with good surface finish.
- Evaluate the models obtained with the physical experiments.
- Test the mechanical strength of the parts obtained through the experiments.

Chapter 3

Background

The author has earlier conducted a project work on the same subject as this thesis named *Closed Form Net Shape Processing of Composites*. Experiments and results from the project that are being discussed in this thesis is described in Appendix D. The objective of the project work was to investigate the *Same Qualified Resin Transfer Moulding* - technique. The flat plate moulding tool and pressure pot described in Chapter 7 were built during the project work. Due to the lack of documentation of the technique in the literature[1] the author had to develop the technique more or less from scratch. The project work found that structurally sound laminates[2] were achievable, but surface quality was quite poor due to air inclusions and precipitated volatiles. The quest to achieve immaculate surface quality will be followed in this thesis.

[1] Only a vague outline is given in ref. [6].
[2] The void content found in the laminates were low.

Chapter 4

Theory

4.1 Composite materials

The composite materials addressed in this thesis are continuos fibre reinforced thermoset polymers. Carbon fibre reinforced epoxy prepreg[1] was used for experiments and calculations.

Important production techniques

The industry standard on prepreg part production is autoclave vacuum bagging. In this method the prepreg is placed on a mould tool (male or female) and bagged with numerous of different plies. This tool accurately predict one side of the part. A vacuum is drawn and the whole assembly is heated in the autoclave. The autoclave also exerts external positive pressure on the tool by a pressurized atmosphere in the autoclave. In order to avoid autoignition due to high partial oxygen pressure, nitrogen is often used in the atmosphere [9]. The vacuum in the bag is often altered

[1] Material product designations:

- *HexPly® 6376C-905-36%* [7], meaning 6376 resin with 905 weave
- *ACG LTM®16* [8]

after the desired autoclave pressure is reached. Some times it is raised to a slight negative pressure. It can also be raised to a substantial positive pressure as long as the external autoclave pressure is higher than the internal bag pressure [10, Chap. 6]. The initial vacuum favors air and volatile evacuation. When the resin gels the external pressure added helps the persisting volatiles to stay in solution. In addition to pressure, the temperature in the autoclave is of key importance. Special temperature schemes are followed. A specific temperature ramp is specified for both the heating and the cooling process. In between, a variety of temperature dwells are added. Only one dwell is common for net resin systems. For systems with excessive resin a dwell is added on lower temperatures allowing the resin to bleed out before the curing dwell starts after a new temperature ramp. A pressure/temperature sequence is illustrated in Figure 4.1.

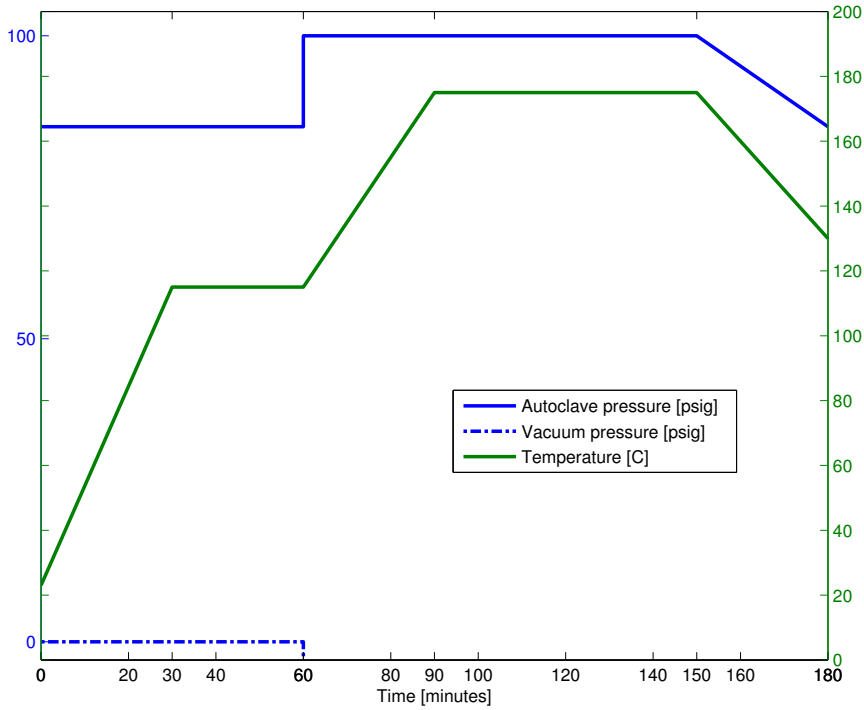

FIGURE 4.1: Illustrative autoclave curing scheme.

In an autoclave consolidation system the resin pressure in the prepreg is elevated

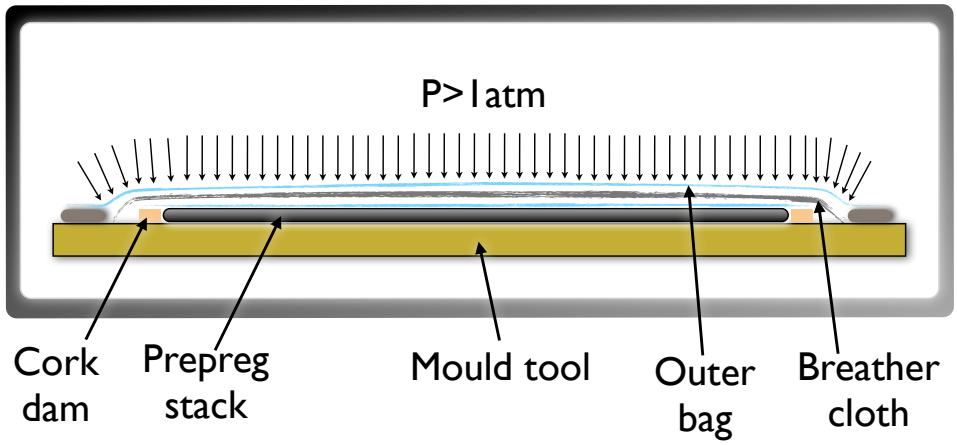

FIGURE 4.2: The principle of the autoclave is illustrated. The black square resembles the autoclave that contains a pressurized atmosphere and the mould tool with prepreg stack and consumable plies attacked. The pressurized atmosphere compresses the fibre stack and elevates the resin pressure.

as a consequence of the autoclave pressure. The system is outlined in Figure 4.2. As Campbell [10, Chap. 6] describes: resin pressure is controlled only indirectly in the system. When heat is applied to the fibre stack the resin viscosity decreases

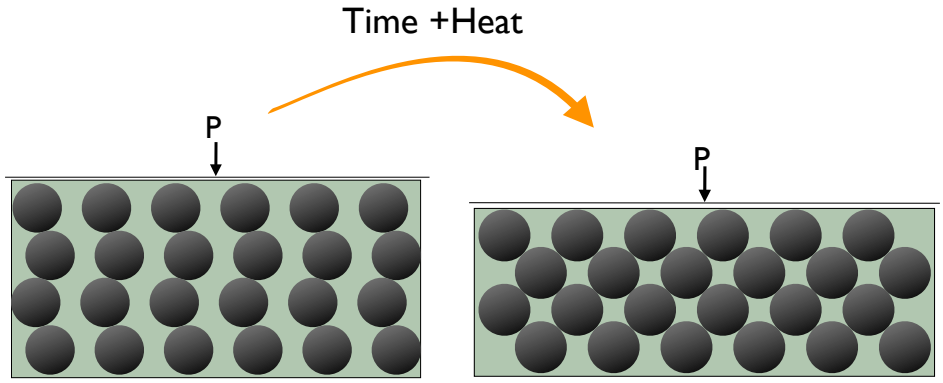

FIGURE 4.3: The figure shows a cross section of a unidirectional prepreg stack. As the resin temperature increases the viscosity of the resin drops dramatically. The pressure compresses the fibre stack and pushes the resin out. The pressure carried by the fibre bed increases.

dramatically. This allows the pressure to compress the fibre stack as described in Figure 4.3. When the fibre strands gets closer to each other the load carrying capability of the fibre stack increases. This leaves less pressure for the resin.

SQRTM theory

In the SQRTM method a stack of prepreg plies, called a preform, is placed inside a closed mould cavity and cured by heating of the tool. Resin is injected simultaneously. The authors understanding of the process is described in detail in Chapter 6.

Resin is injected in to the mould cavity in order to increase the resin pressure. The resin pressure is in that manner controlled hydrostatically. The physical property of permeability is important in a SQRTM setup. The permeability of a fibre bed describes the resistance of flow through it. High permeability yields high flow and vice versa. This relation is described by Darcy's law,

$$\mathbf{v} = -\frac{\mathbf{K}}{\mu}\nabla p \tag{4.1}$$

her $\mathbf{v}$ is the velocity vector , $\mathbf{K}$ the permeability tensor, μ the viscosity and ∇p is the pressure gradient. In the LCM field the permeability definition used has the unit of [Length^2], this evolves from Darcy's law (Equation 4.2). Other fields of interest, as for instance soil consolidation problems, often define the permeability with the unit of [Length $\cdot$ Time^{-1}]. The latter is by some authors referred to as the *hydraulic conductivity* of the porous medium [11]. The conversion between the two is $\mathbf{K} = \frac{\nu}{g}\mathbf{k}$, where $\mathbf{K}$ is the permeability, ν is the dynamic viscosity, g is the acceleration of gravity and $\mathbf{k}$ is the hydraulic conductivity. Due to this difference care has to be taken when using FEA codes addressing the matter. The ABAQUS code used in this work uses both definitions dependent on which module is used for the calculation. As the conscious reader might understand the property of permeability was not natively used for fibre beds. Darcy, for instance, found his law studying seepage of fluid through a granular medium [12, p.144]. For isotropic media consisting of spherical objects, the permeability can be estimated by analytical expressions with regards on porosity[2] However, for anisotropic media

[2]Porosity is in this context defined as the volume fraction of empty space inside the media. (often denoted by ϵ).

like fibre beds (not consisting of spherical objects) permeability has to be found by empirical tests. One has to distinguish between saturated and unsaturated permeability. For the SQRTM case, where the preform is always saturated the saturated permeability is the one of main interest. Kruckenberg and Paton [1] describe a fairly easy way to determine the saturated permeability. It consist of a fibre bed debulking tool with a transparent lid. It has edge inlets and outlets and thus yields unidirectional flow. The pressure difference and volume flow is measured. The results are ploted as in Figure 4.4 and the permeability is found through the use of a scalar form of Darcy's law as in Equation (4.2). Where v is the average velocity, Q the volume flow, A the area of the flow, K_e^θ is the effective permeability and $\frac{\Delta P}{L}$ resembles the pressure gradient over the porous medium. L is the length of the flow. As seen in Figure 4.4 volume flow through a porous medium is linearly dependent on pressure . This relation is provided that viscosity and fibre fraction is kept constant. Through linear interpolation (indicated by the black lines) and simple analytical operations an effective permeability K_e^θ can be found. However for prepreg preforms the viscosity is very high if the temperature is kept at room temperature and for elevated temperatures the resin gels due to curing. This greatly complicates the tests as viscosity will change rapidly.

$$v = \frac{Q}{A} = \frac{K_e^\theta}{\mu}\frac{\Delta P}{L} \tag{4.2}$$

Laminate theory (All equations from Kollár and Springer [13].)

A cured part of composite material is characterized as a laminate. A laminate consists of one or more plies. In a prepreg laminate each ply consists of a cut out of the prepreg roll. The fact that plies can vary orientation according to the application enables highly strength effective parts. The elastic behavior of such laminates are governed by the classical laminate theory. The laminate theory will be outlined next.

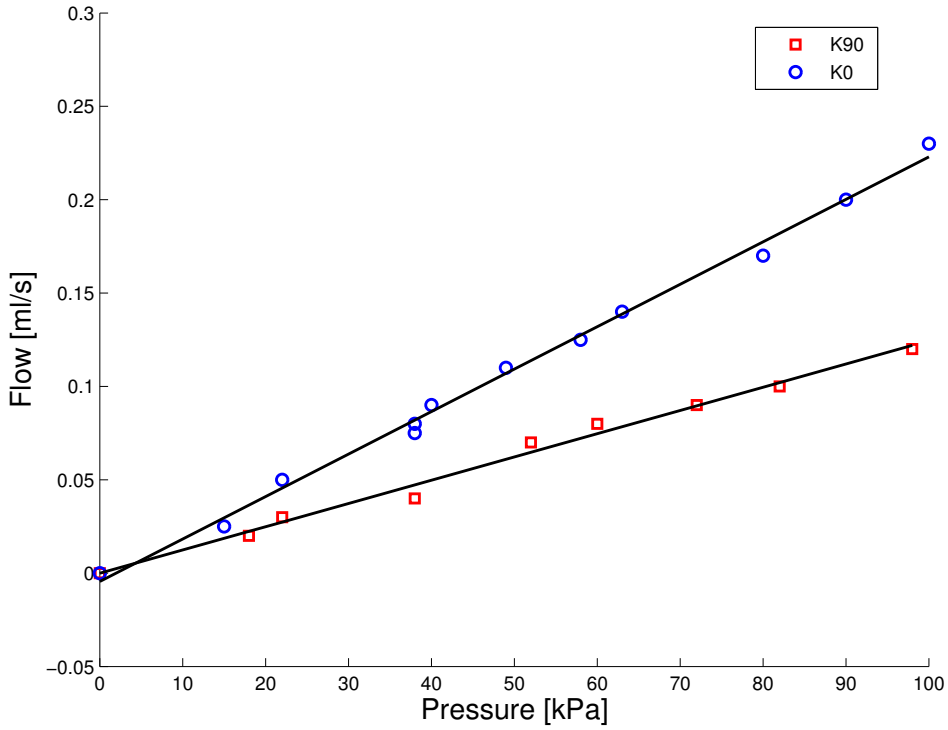

FIGURE 4.4: The results from a saturated permeability test. K0 is the results for 0-direction and K90 is the results for the 90-directon. Adapted from [1]

Hook 's law for anisotropic material shows the relation between stresses and strains as shown in Equation (4.3).

$$\begin{Bmatrix} \sigma_1 \\ \sigma_2 \\ \sigma_3 \\ \tau_{23} \\ \tau_{13} \\ \tau_{12} \end{Bmatrix} = \begin{bmatrix} C_{11} & C_{12} & C_{13} & C_{14} & C_{15} & C_{16} \\ C_{21} & C_{22} & C_{23} & C_{24} & C_{25} & C_{26} \\ C_{31} & C_{32} & C_{33} & C_{34} & C_{35} & C_{36} \\ C_{41} & C_{42} & C_{43} & C_{44} & C_{45} & C_{46} \\ C_{51} & C_{52} & C_{53} & C_{54} & C_{55} & C_{56} \\ C_{61} & C_{62} & C_{63} & C_{64} & C_{65} & C_{66} \end{bmatrix} \begin{Bmatrix} \epsilon_1 \\ \epsilon_2 \\ \epsilon_3 \\ \gamma_{23} \\ \gamma_{13} \\ \gamma_{12} \end{Bmatrix} \tag{4.3}$$

Where the $[\mathbf{C}]$ matrix is the stiffness matrix and its inverse $[\mathbf{S}] = [\mathbf{C}]^{-1}$ is the compliance matrix. σ_i and τ_{ij} are normal and shear stresses and ϵ_i and γ_{ij} are normal and shear strains. According to Kollár and Springer [13, p.11] it can be

shown that both the stiffness and the compliance matrix are symetrical for elastic materials. Hence, there are 21 independent elastic material constants.

The laminate system consists of plies that are stacked in to laminates. For each ply there is a coordinate system denoted x_1, x_2, x_3 , this is the local ply coordinate system. Accordingly, for each laminate there is global laminate coordinate system-denoted x, y, z . The laminate theory transforms the properties of each ply in to the global coordinate system and summarizes these properties in order to obtain the properties of the whole laminate. The following assumptions are taken:

Assumptions of the classical laminate theory [14]

- Plane stress state
- Strains vary linearly through the thickness
- Strains and displacements are linearly related
- Displacements are small compared to the thickness of the laminate
- Out of plane normal strains and shear strains are neglected
- Normal distance from any point to the middle surface remain constant
- Materials have linear elastic behavior.

The plane stress assumption implies that one of the normal stresses or two of the shear stresses are zero. Each ply has theire respective stiffness matrices $[Q_k]$ in the local coordinate system. This yields for each ply the stress-strain relation in Equation (C.5)

$$\begin{Bmatrix} \sigma_1 \\ \sigma_2 \\ \tau_{12} \end{Bmatrix} = \begin{bmatrix} Q_{11} & Q_{12} & Q_{16} \\ Q_{12} & Q_{22} & Q_{26} \\ Q_{16} & Q_{26} & Q_{66} \end{bmatrix} \begin{Bmatrix} \epsilon_1 \\ \epsilon_2 \\ \gamma_{12} \end{Bmatrix} \tag{4.4}$$

For each ply the properties are transformed in to the global coordinate system by applying Equation (4.5)

$$[Q'_k] = [T_\sigma]^{-1}[Q_k][T_\epsilon] \tag{4.5}$$

Where $[Q'_k]$ is the transformed stiffness matrix and $[T_\sigma]$ and $[T_\epsilon]$ the transformation matrices,

$$[T_\sigma] = \begin{bmatrix} c^2 & s^2 & 2cs \\ s^2 & c^2 & -2cs \\ -cs & cs & c^2 - s^2 \end{bmatrix}, [T_\epsilon] = \begin{bmatrix} c^2 & s^2 & cs \\ s^2 & c^2 & -cs \\ -2cs & 2cs & c^2 - s^2 \end{bmatrix} \tag{4.6}$$

Here, s and c denotes $\sin(\theta)$ and $\cos(\theta)$. The angle θ is depicted in Figure 4.5a. Now the summation of the different ply properties are executed as follows,

$$\begin{aligned} \mathbf{A} &= \sum_{k=1}^{n} \mathbf{Q'}_k (h_k - h_{k-1}) \\ \mathbf{B} &= \frac{1}{2} \sum_{k=1}^{n} \mathbf{Q'}_k (h_k^2 - h_{k-1}^2) \\ \mathbf{D} &= \frac{1}{3} \sum_{k=1}^{n} \mathbf{Q'}_k (h_k^3 - h_{k-1}^3) \end{aligned} \tag{4.7}$$

Here, h_k is the z-coordinate on the topside of each ply, accordingly h_{k-1} is the bottom coordinate. Through this approach the stacking sequence of each ply in relation to the geometrical mid-plane of the laminate is accounted for. The stacking sequence can be seen in Figure 4.5b.

The $[\mathbf{A}]$, $[\mathbf{B}]$ and $[\mathbf{D}]$ matrices are the constituents in the laminate stiffness matrix (LSM) which can be used to calculate in-plane laminate stresses and strains as followed,

$$\begin{Bmatrix} N_x \\ N_y \\ N_{xy} \\ M_x \\ M_y \\ M_{xy} \end{Bmatrix} = \left[\begin{array}{ccc:ccc} A_{11} & A_{12} & A_{16} & B_{11} & B_{12} & B_{16} \\ A_{12} & A_{22} & A_{26} & B_{12} & B_{22} & B_{26} \\ A_{16} & A_{26} & A_{66} & B_{16} & B_{26} & B_{66} \\ \hdashline B_{11} & B_{12} & B_{16} & D_{11} & D_{12} & D_{16} \\ B_{12} & B_{22} & B_{26} & D_{12} & D_{22} & D_{26} \\ B_{16} & B_{26} & B_{66} & D_{16} & D_{26} & D_{66} \end{array}\right] \begin{Bmatrix} \epsilon_1^0 \\ \epsilon_2^0 \\ \gamma_{xy}^0 \\ \kappa_x \\ \kappa_y \\ \kappa_{xy} \end{Bmatrix} \tag{4.8}$$

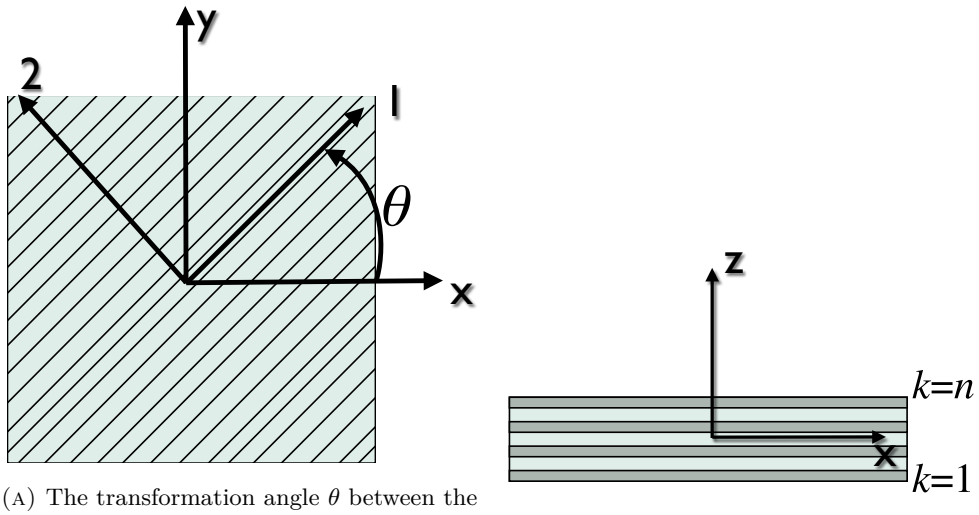

(A) The transformation angle θ between the global and the local coordinate system displayed.

(B) The stacking direction and number sequence of the plies is here depicted.

FIGURE 4.5:

Here, N_i is in-plane normal forces, N_{ij} in-plane shear force, M_i is bending moment around the axis indicated and M_{ij} is twist. All elements on the left hand side of the equal sign is per unit length. On the right hand side the deformations are given. ϵ_i and γ_{xy} are in-plane strains and the κ are out of plane curvature of the laminate. The zero in ϵ_i^0 indicates that the strains are evaluate at the geometrical mid-plain of the laminate. To find strains in the respective plies the following relation is applied,

$$\begin{Bmatrix} \epsilon_1' \\ \epsilon_2' \\ \gamma_{xy}' \end{Bmatrix} = \begin{Bmatrix} \epsilon_1^0 \\ \epsilon_2^0 \\ \gamma_{xy}^0 \end{Bmatrix} + z \begin{Bmatrix} \kappa_x \\ \kappa_y \\ \kappa_{xy} \end{Bmatrix} \tag{4.9}$$

Where z is the distance from the geometrical mid-plane and ϵ_i is the normal strain in the corresponding plane (laminate coordinate system). It is possible to obtain stresses for the different plies by retracing the rout of calculation. First the strains from Equation (4.9) have to be transformed in to the local ply coordinate system,

$$\begin{Bmatrix} \epsilon_x \\ \epsilon_y \\ \gamma_{xy} \end{Bmatrix} = \begin{bmatrix} c^2 & s^2 & cs \\ s^2 & c^2 & -cs \\ -2cs & 2cs & c^2 - s^2 \end{bmatrix}^{-1} \begin{Bmatrix} \epsilon'_x \\ \epsilon'_y \\ \gamma'_{xy} \end{Bmatrix} \tag{4.10}$$

Now, by reapplying Eq. (C.5) the in-plane stresses for a certain ply can be found in the ply coordinate system.

Void formation and curing

Voids are holes or bubbles in the laminate where resin is not present. They pose a threat to the mechanical integrity of the laminate as they serve as stress concentration sites. Olivier et al. [15] show that transverse tensile strength can drop as low as 70% of its primary value if a void content of 10% is introduced in the laminate (UD). The longitudinal tensile strength is far less affected. Voids form in different ways. Volatiles and entrapped air are known initiators. Voids can form both intralaminar (inside a fibre tow or ply) and interlaminar (in the intersection between plies)[10]. If the hydrostatic resin pressure is higher than the vapor pressure of the volatiles, the volatiles will remain in solution in the resin throughout the cure and voids will not form [15]. This is an important reason why high resin pressure should be applied.

The resin used in carbon fibre applications are often epoxy based (other resins, like bismalemid, polyester and vinylester are also used). Epoxies can be bought both as one and two component systems. In the two component systems the base resin is mixed with a curing agent. The curing agent allows the polymer chains in the resin to cross link and form one large molecule. The one component systems already contain the curing agent and it is activated through heat. One component resins are used in prepregs. The reactive epoxy group can be seen in Figure 4.6. The chains are cross linked when the oxygen bonds are split open and connected to the curing agent.

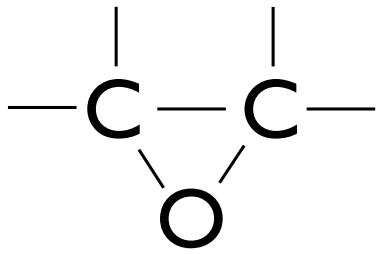

FIGURE 4.6: The characteristic epoxy group. It can be situated on a variety of different molecules.

4.2 Three point bending

In a three point bending test the laminate is tested by adding load to a specimen that rests on two side supports. A possible method is illustrated in Figure 4.7.

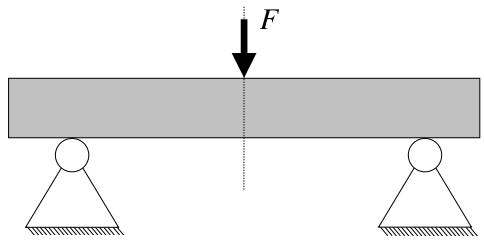

FIGURE 4.7: In a three point bending test the laminate specimen is loaded in the center and allowed to rotate around the supports.

Wisnom [16] explains that the method used for deduction of results from a three point bending test assumes a parabolic shear stress distribution across the specimen cross section. This is valid only for linear elastic material models. Davies et al. [17] use the three point bending method described in ASTM D2344M to establish the ILSS of a unidirectional laminate. This short beam method[3] favors high shear stresses in the laminate and is thus suited to determine shear strengths of a laminate. However, care has to be taken as the experienced failure mode may vary [18].

[3] A short beam test is a three point test with a short specimen.

4.3 Modeling of flow in porous media (CFD)

ABAQUS 6.12 was used for porous media flow simulations. In this code porous media flow is governed by the Brinkman-Forchheimer equation (Equation (4.11) from [11]):

$$\frac{\rho}{\epsilon}\left[\frac{\partial \mathbf{v}}{\partial t} + \mathbf{v}\cdot\nabla\left(\frac{\mathbf{v}}{\epsilon}\right)\right] = -\nabla p + \frac{\mu}{\epsilon}\nabla\cdot\nabla\mathbf{v} - \frac{\mu}{K}\mathbf{v} - \frac{\rho C F}{\sqrt{K}}|\mathbf{v}|\mathbf{v} \tag{4.11}$$

Here $\mathbf{v}$ is volume averaged velocity, p is volume averaged pressure, ρ is the density of the fluid, μ is the viscosity of the fluid, ϵ is the porousity (the volumfraction of matrix) and K the permeability of the porous material. Brinkman -Forchheimer is a general form of Darcy's law [1] as described in Equation(4.1) as it accounts for inertia effects and solid wall boundaries.

The ABAQUS code has the following limitations in porous media flow [11]:

- Incompressibility ($\nabla\cdot\mathbf{v} = 0$)
- Porosity can not vary with time.
- Permeability is isotropic and varies with the porosity of the medium.

According to White [19, p.19] incompressibility is a good assumption for most liquids as their density vary little with pressure. Also, the fibre preform has constant porosity as long as the tool is closed during the simulation step. Hence, the two first limitations are good approximations. The latter limitation does not fit with reality. According to Kruckenberg and Paton [1] the through-thickness-permeability of a fiber bed is in the range of 10%-20% lower than the in-plan permeabilities. Measures were taken to overcome the inconvenience of the limitation. This is described in Chapter 5.

Chapter 5

Porous media modeling

The nature of pressure distribution and resin flow inside the prepreg preform is what distinguishes SQRTM from other prepreg moulding methods. The placing of vents and inlets is paramount for the process outcome. Through inlets and vents the engineer is able to control resin pressure directly. However, the flow in porous media is not trivial to understand and computational fluid dynamics simulations for flow in porous media have been done with the ABAQUS 6.12 software. There are numerous of commercial codes available for resin flow in dry fibre preforms, though process control is limited to the parameters necessary for the RTM method as the calculations stops when the preform is fully saturated. In those known to the author[1], that is. When a new production method is developed the constraints should not be limited by the software and that is why ABAQUS was used.

The numerical model obtained consists of a fluid filled volume that is dimensionally identical to the mould cavity used in the experiments. This fluid volume contains a permeable media saturated in a liquid. Viscosity and permeability properties are assigned to the volume. By this approach resin flow and pressure distribution in the mould cavity was investigated.

[1] *RTM-worx* and *Autodesk mould flow designer* was tested during the project work

5.1 Verification of the simulation method

An ABAQUS verification example[2] was used to see that the model yielded the appropriate results. First the example, as seen in Figure 5.1a, was calculated. A fully developed stream enters on the left hand side and a pressure of 0 bar is constrained on the right. No slip conditions were applied on the top and bottom surfaces. The only boundary conditions for the in-plane walls were zero velocity through the wall, this enforces a 2D behavior on the model. Data was collected throughout the length of the path shown in Figure 5.1b.

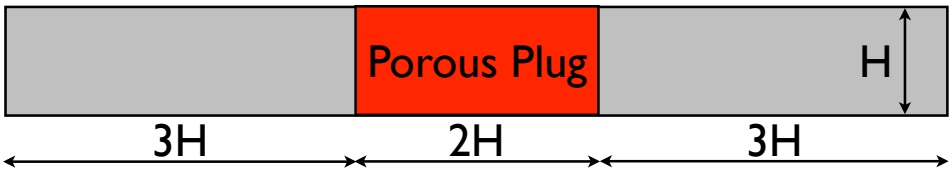

(A) The porous plug from the ABAQUS manual. The red section resembles the porous region. Adapted from [11]

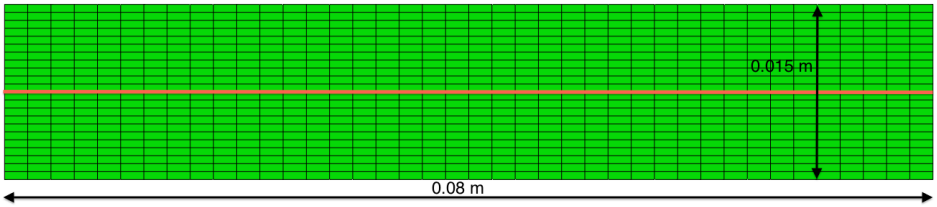

(B) The figure depicts the 40×22 fluid mesh used in the analyses. The red line indicates the path from which data were collected. A porous section is defined in the middle.

(C) The velocity in the channel is depicted. Red is higher velocity.

FIGURE 5.1:

[2]The example was picked from the ABAQUS verification manual chapter 3.3.5. See ref. [11] for the manual

The publisher verified the ABAQUS code on this problem by comparing the result with a paper by Betchen and Thompson [20]. The results obtained by running the .inp-file attached in the manual can be seen in Figure 5.1c and 5.2

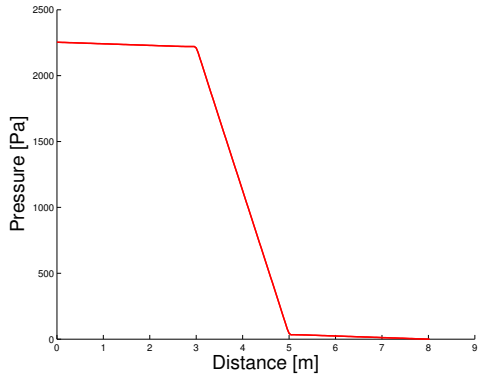

(A) Pressure – Distance plot for the example problem.

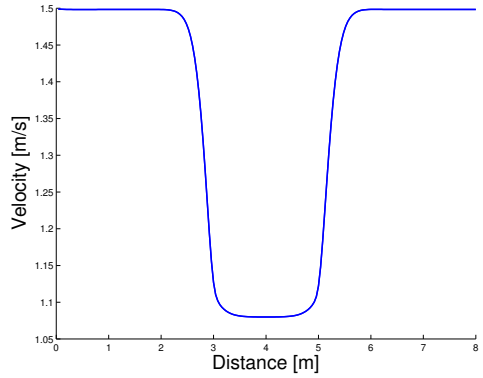

(B) Velocity – Distance plot for the example problem.

FIGURE 5.2:

A similar test was modeled and calculated for the parameters applicable for the SQRTM case. A mesh refinement procedure was carried out. The result of this is shown in Figure 5.3. The different meshes gives reasonably similar results for the pressure plot. For the velocity case however, few elements gives huge discrepancies. A mesh corresponding to the 101×76 mesh was therefor used.

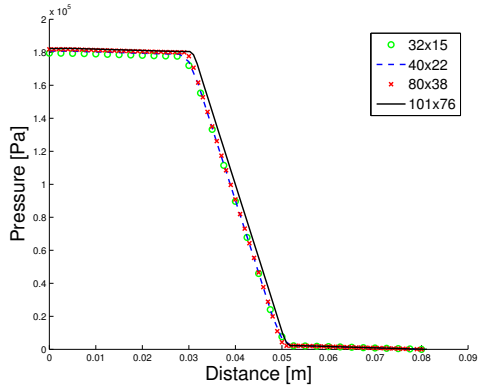

(A) Pressure – Distance plot for the SQRTM relevant problem.

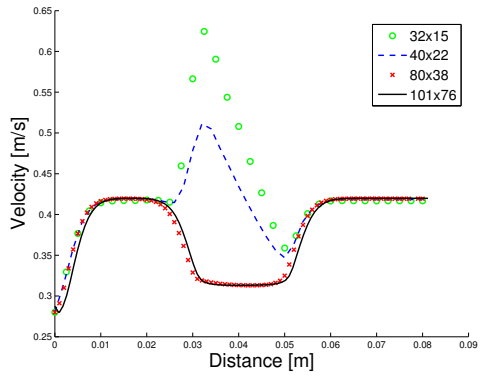

(B) Velocity – Distance plot for the SQRTM relevant problem.

FIGURE 5.3:

5.2 The SQRTM model

By utilizing this knowledge a model of the whole system was built. The model was isothermal with incompressible flow and the eight node brick element *FC3D8* was used. The FC3D8 element is a continuum element that allows fluids to flow through it. A porous media section identical to the mould cavity was modeled. Unfortunately the permeability of a porous section is restricted to be isotropic in the ABAQUS code. For the fiber preform this is a good assumption in the in-plane directions, but the through-thickness direction has a lower permeability. Sections of lower permeability were added in the inlet and outlet of the cavity in order to overcome this limitation. Here, and only here, is the out of plane resin flow assumed to be important. The limitation is in that manner omitted.

Boundary conditions

Due to symmetry only half of the model was meshed. (Depicted in Figure 5.4). The following boundary conditions were applied to the model:

- Inlet: $\mathrm{P} = 7\,\mathrm{bar}$
- Outlet: $\mathrm{P} = 0\,\mathrm{bar}$
- Symmetry plane (xz-plane): $V_y = 0\,\mathrm{m\,s^{-1}}$
- Walls and other surfaces: no slip (meaning $V_x = V_y = V_z = 0$)

Mesh size validation

As seen in the Figure 5.3b the results obtained can vary dramatically if a wrong mesh is fitted. Therefore, a mesh refinement procedure was carried out. The results were obtained from a straight line in the symmetry plane in-between the inlet and outlet and can be seen in Figure 5.5. The chosen mesh had four elements through the thickness and a total of 2800 elements.

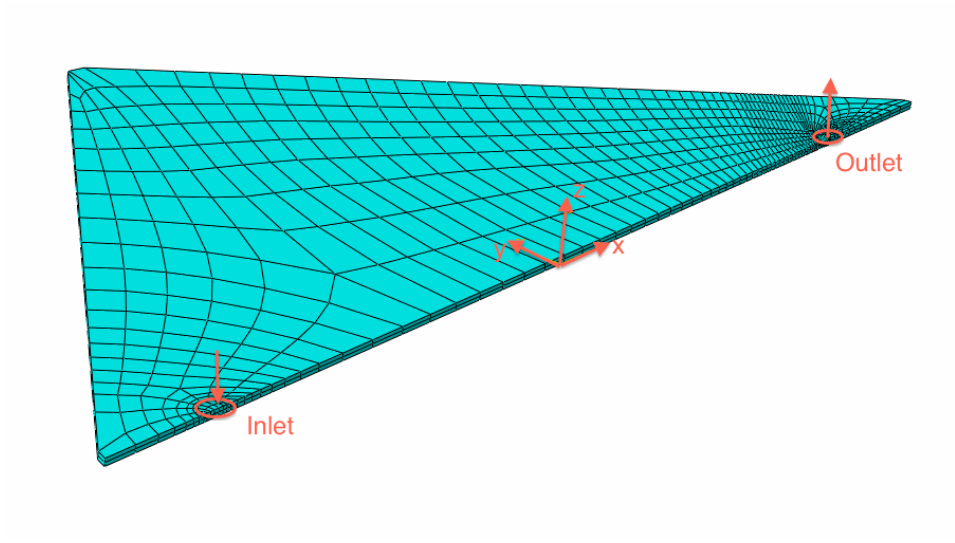

FIGURE 5.4: The model of the SQRTM system cut in the plane of symmetry with the WCS showed. The FC3D8 mesh is fitted.

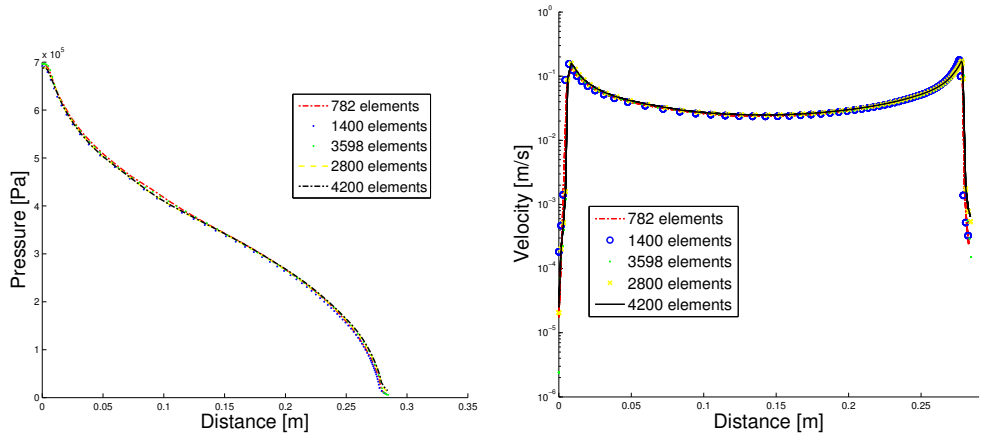

(A) Pressure – Distance plot for the SQRTM model.

(B) Velocity – Distance plot for the SQRTM model.

FIGURE 5.5:

Velocity and pressure field

As described by Darcy's law (in Chapter 4) the relation between the pressure gradient and the flow velocity is dependent on the permeability of the fibre bed and

the viscosity of the wetting liquid. Due to the fact that accurate permeability measurements are hard to achieve and that the preform permeability is kept constant due to constant fibre volume fraction no permeability tests were conducted in this study. Hence, all the permeability numbers used in this report are retrieved from other authors. While permeability is constant, viscosity vary greatly with both time and temperature. Viscosity – Time plots for the 6376-resin were found in the paper by Davies et al. [17]. The data is presented in Figure 5.6. These data were used to predict the change in viscosity in order to simulate the rate of change in pressure and velocity in the cavity. Successive simulations were run with different viscosities in the wetting liquid. The results can bee seen in Figure 5.7.

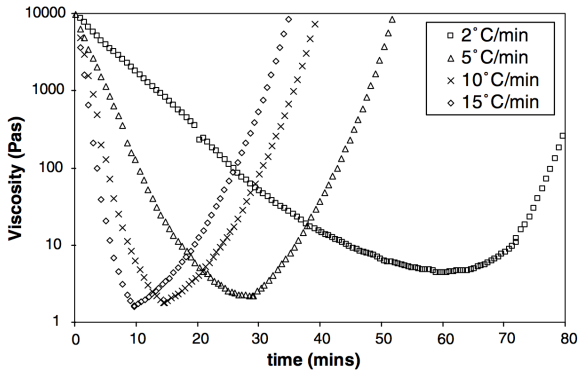

FIGURE 5.6: The plot shows the viscosity of neat 6376-resin as a function of time at a given heat up rate. Adapted from [17].

The simulation shows that the pressure and the pressure gradient through the preform is independent of the viscosity. It also shows that the velocity of the flow is inversely proportional to the viscosity. The latter is supported by Darcy's law.

To further comprehend the relation between viscosity and velocity a new plot was deduced analytically. By rearranging Darcy's law and divide by the length of the flow, the Time – Length plot in Figure 5.8 is obtained. The Matlab calculations can be seen in Appendix A. From the calculations and simulations it is evident that the viscosity of the resin has to be lowered if one is dependent on movement of the resin. Small gaps will often persist in the mould cavity before heating, hence the resin will have to fill these. For an elevated resin pressure however one do not need

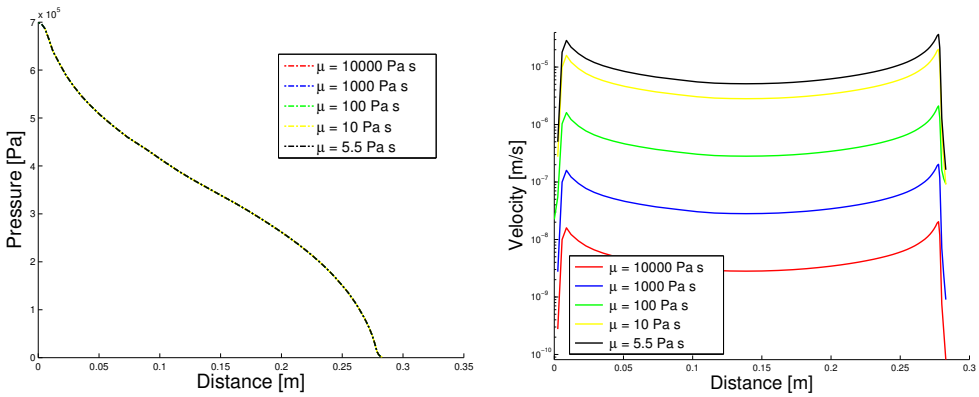

(A) Pressure-Distance plot with different viscosities. All plots are coincident.

(B) Velocity-Distance plot with different viscosities.

FIGURE 5.7:

a lower viscosity. Nevertheless, hydrostatic pressure distribution is only possible if no gaps or bubbles are present in the resin. Therefore, a lowered resin viscosity will be necessary in most cases.

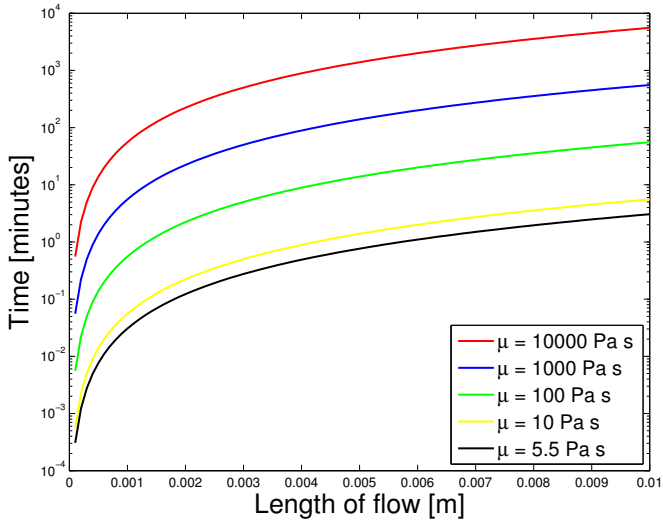

FIGURE 5.8: The plot describes how far a flow has moved in a saturated preform after a certain time and a given viscosity. Values used are $K = 3 \times 10^{-7}\,\mathrm{cm}^2$ and $\Delta P = -1\,\mathrm{bar}$.

Chapter 6

Interpretation of the SQRTM-method

It is important to understand the SQRTM techniques way of working in order to conduct the correct experiments. The basic understanding of the process prior to the execution of the experiments, based on references in the literature and sound engineering practice, is presented next.

Process steps[1]

1. Preform debulking
2. Laminate compression
3. Resin injection
4. Curing
5. Demoulding

[1] The steps in the enumerated list are deduced from earlier results [27]

Preform debulking

There are two reasons for thorough execution of this step. One is the volatiles that are contained within the resin, these will evaporate at a given temperature and emerge to the mould surface. Here they will form surface voids if they are not removed before the resin gels. This removing mechanism has proven hard do achieve in the SQRTM-setup. It might be hard not to entrap any air when the preform is assembled in to the mould tool. The preform debulking can either be done by hand or with the application of a vacuum bag. For the best possible debulk action the vacuum bag method is preferred as it both provides a mechanical compression force and a pressure gradient that favors evacuation of air. For the evacuation of volatiles prior to tool closing a hot preform debulk is possible.

In autoclave part production a room temperature vacuum hold is often used on the prepreg stack. This can be done both to evacuate air that is entrapped between the plies and air between the tool and the fibre stack [21, 22]. The latter to ensure good surface finish. This vacuum debulking procedure can be applied multiple times throughout the layup procedure. For a versatile production method subsequently compacting the fibre stack by hand should suffice for good surface finish and low void content. When the production process is unfamiliar a proper vacuum debulk can be applied in order to facilitate the best possible outcome. Such an conservative approach was proposed by the industry [23], consisting of 5 min room temperature vacuum hold between each ply and a 10 min vacuum hold at 60 °C. Both methods were tested during the experiments.

Laminate compression

The closing action of the mould tool executes this step. After the debulk is done the preform thickness is still greater than the mould cavity. The closing of the tool compresses the preform to maintain the final laminate thickness. This can either be done with a great force at room temperature or with a lower force at elevated temperatures as the viscosity of the resin decreases. This was shown by Lukaszewicz

and Potter [24] in compression tests of uncured prepreg. However, the preform compaction is governed by two different mechanisms. One is the compression of the resin (where the viscosity is important) and one is the compaction of the fibre bed. As the fibre volume fraction (v_f) increases the fibre bed takes more of the load and for extreme fibre volume fractions the compression force is predicted by the fibre bed compaction alone [10]. As opposed to conventional matched mould methods where the closing action and compression of the tool yields elevated resin pressure, the closing action of the tool in SQRTM posses only the functions of defining the laminate thickness (and hence, the fibre volume fraction of the laminate) and attaining a sealed mould cavity. As a consequence the mould cavity was designed to obtain a sound fibre volume fraction. The ply thickness was predicted using Figure 6.1.

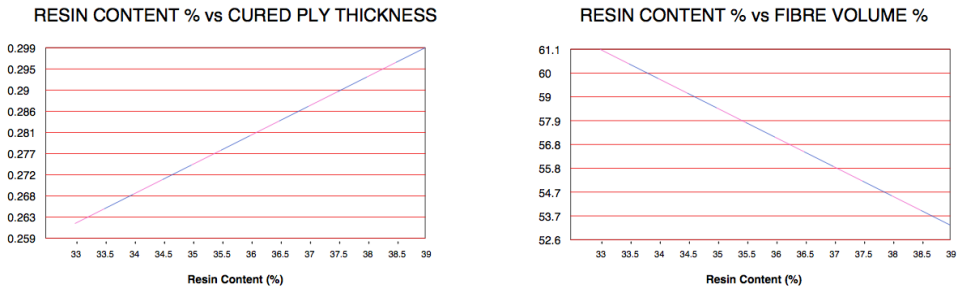

FIGURE 6.1: The figure shows the relation of ply thickness, resin content and fibre volume fraction of the prepreg used. A cavity hight of 2.2 mm containing eight plies yields a volume fraction of approximately 58 %. Adapted from [7].

Resin pressure

Resin is injected in to the mould cavity in order to elevate the resin pressure therein. While the debulking step removes as much as possible of the volatiles and air bubbles, the resin injection step seek to keep volatiles in solution. If an elevated hydrostatic resin pressure is achieved the laminate can be virtually void free. According to Olivier et al. [15] a curing pressure raised above 7 bar does not decrease void content noticeably in comparison to a 7 bar pressure cure. For autoclave cure that is.

As Olivier et al. [15] show, the key to excellent laminate quality is elevated resin pressure. This facilitates both good surface finish and low void content. The nature of SQRTM implies utilization of external resin injection in to the cavity. This enables distinct resin pressure control. The resin injection can be accomplished through different solutions. A piston – barrel assembly is widely used in the industry [25]. Other possibilities are inert gas pressure chambers or blather/diaphragm container assemblies compressed by pressurized gas or liquid. The system used in this work was a pressure chamber using pressurized air for compression of the resin. This solution provided a 7 bar resin pressure when the standard workshop air was used directly. The system featured easy cleaning and a minimum of disposals as well as a cost effective purchase. It was well suited for small scale testing. In the execution of the experiments care has to be taken in order to obtain a hydrostatic resin pressure. This is only achieved if the entire cavity is filled with resin (meaning a minimum of air bubbles). The vent and sprue included. The sought practice in the experiments was therefor to let resin flow through the vacuum vent before the vent was closed.

Curing

All the above steps contribute to obtain a best possible cured part. When all the necessary precautions are taken the cure is dependent on the heating cycle alone. The main objective of the heating cycle is to cross-link the resin in order to cure it. Another important objective for the heating is to facilitate resin flow between the different plies in the preform and tool surface. As the viscosity decreases with the elevated temperature it allows the resin to fill voids and blend with the resin from the other plies. According to Davies et al. [17] a heating cycle that favors this low viscosity flow provides mechanically stronger laminates than those who don't. It is shown that different cure cycles effects the inter laminar shear strength of the laminate [17]. A basic, single dwell cure cycle was chosen for the experiments executed. This was both easy to implement and to comprehend. The cure cycle used was the one recommended by Hexcel [7] (seen in Figure 6.2a).

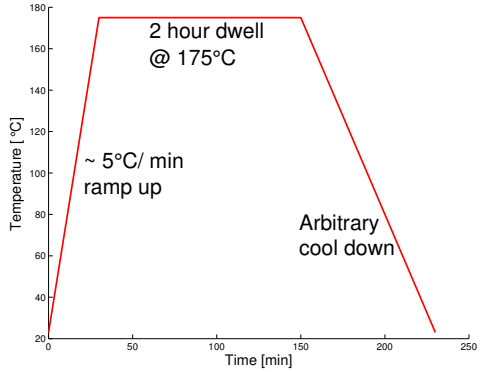

(A) The basic cure cycle used in the experiments is shown in the figure.

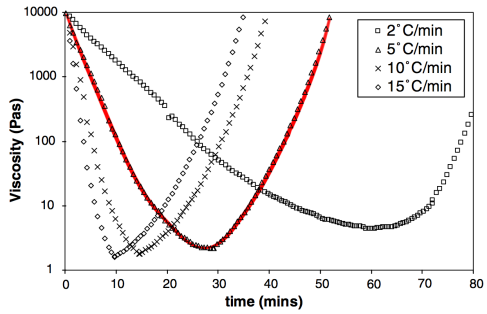

(B) Viscosity – Time plot for the 6376-resin. Red line indicates the rehology for the intended cure cycle. Adapted from [17]

FIGURE 6.2:

The rehology depicted in Figure 6.2b was used to predict the resin behavior inside the mould tool. As perviously shown in Chapter 4 the viscosity has a large effect on the velocity of the flow. Hence, outflow of the mould was expected in the low-vicosity area.

Demoulding

The part is not moulded until it is demoulded. Challenges might occur in this step if both the cure temperature of the resin system and the CTE of the tool is high. The part can get stuck inside the tool and either the part or the tool can get damaged. If the parts are thin and small, buckling of the cured part might be eligible upon cool down. Buckling can be omitted if demoulding is done at elevated temperatures. Either way, some sort of ejection mechanism is clever to integrate in to the tool.

According to technical data sheet [7] the glass transition temperature of a 6376-laminate is 196 °C after the aforementioned cure cycle. Thus, the part can be demoulded with no cool down. Though, considering the size and thickness of the laminate it was decided that buckling was eligible. Cold demoulding was more easy to achieve as no heat protection was required during the operation. Due to

the fact that the thermal expansion of the mould tool was far greater than the thermal expansion of the fibre bed a substantial compression force was expected to be imposed on the part upon cool down. An ejection mechanism consisting of a threaded hole plugged with a screw was thus implemented in the tool. It was designed for a pressurized air gun nozzle to execute the ejection after the screw was removed.

The considerations presented in this chapter were used to design the process in Chapter 7 and to execute adequate experiments and tests presented in Chapter 8.

Chapter 7

Experimental setup

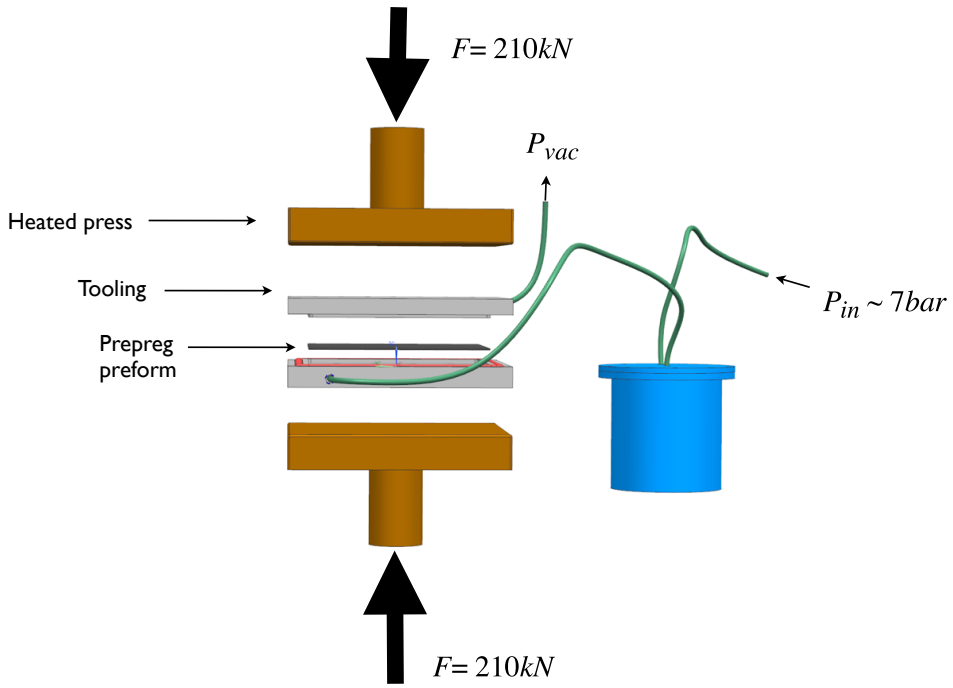

FIGURE 7.1: Illustrative outline of the experimental setup, containing heated platen press, mould tool, resin pressure pot and prepreg preform.

An experimental setup governing the functions in Figure 7.1 has been developed and built. The considerations taken and the finished setup is presented in this chapter.

7.1 Mould tool

In closed mould applications a good tool design is of severe importance. In addition to give the part its correct shape the tool often contains both injection ports, vents, heating/cooling channels and sealing geometry.

Tool rigidity

The tool must be rigid enough to keep the surface shape within the given tolerances. As a result from this tooling cost is greatly dependent on resin pressure. In order to close the tool, some sort of clamping arrangement is needed. Numerous bolts along the circumference of the tool are widely used. Air cushions and platen presses might also be used for this purpose. A heated platen press greatly minimize the amount of functionalities needed in the tooling it self, but this is only suitable for parts of simple geometry and limited size. Dependent on the clamping mechanism chosen the requirements for the structural integrity of the tool changes. A tool with a bolt clamp system will have to withstand huge forces. A resin pressure of 7 bar exerted on a $1\,m^2$ surface need 700 kN of clamping force for the resin pressure alone. In addition comes the fibre debulking force and seal deformation force. On the contrary a platen press system supports the entire outer surface of the tool. This makes the structural integrity requirements for the tool insignificant. Due to the experimental character of the study a platen press was chosen for the setup. It provided both heating and temperature control as well as clamping force. The size limitation of $L^2 = (320\,mm)^2$ was considered to be of minor importance as test specimens of adequate size were possible to produce.

Mould landing and sealing geometry

In order for the mould tool to mould net shaped parts it has to define a given mould cavity that does not depend on clamping force or fibre content. This can easily be achieved through a mould landing geometry that clearly defines when the tool is closed or not. The mould landing geometry should limit the extent of the part in all in-plane directions.

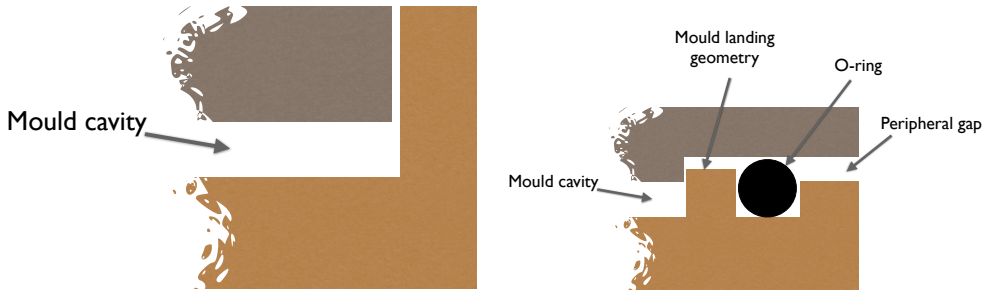

FIGURE 7.2: A badly designed mould that does not properly define the laminate thickness (A). (B) shows a design that both seals the mould and defines the laminate thickness in a controlled way.

There is no need for the tooling halves to land everywhere outside the mould cavity. If a gap is made between the tool halves on the outer periphery this will ease the mould parting. The gap can be measured in order to determine complete mould closing. A large landing flange also makes cleaning in between mould operations more tedious. Nevertheless, the landing geometry need to be capable of enduring the whole clamping force if the tool should be closed with no preform.
The area out side the mould cavity has to contain some sort of sealing. Even though the mould halves are intended to close all around the periphery of the part it requires too tight tolerances to make this geometry seal.

O-rings are widely used for this task, other methods are not discussed here. Due to the peripheral gap sought for the tool the o-rings have to be larger than expected. This is because of an effect called extrusion. A graph describing the effect is provided in Figure 7.3. The gap in the tool was chosen to be 2 mm. Because of the

authors lack of experience with o-rings a large safety factor was introduced and an o-ring of diameter 10 mm was used. The o-ring groove was machined according to tables provided by Otto Olsen AS [26].The o-ring used was of Silicon Shore 60 material [1]. The silicon can withstand temperatures exceeding the required curing temperature of 175 °C.

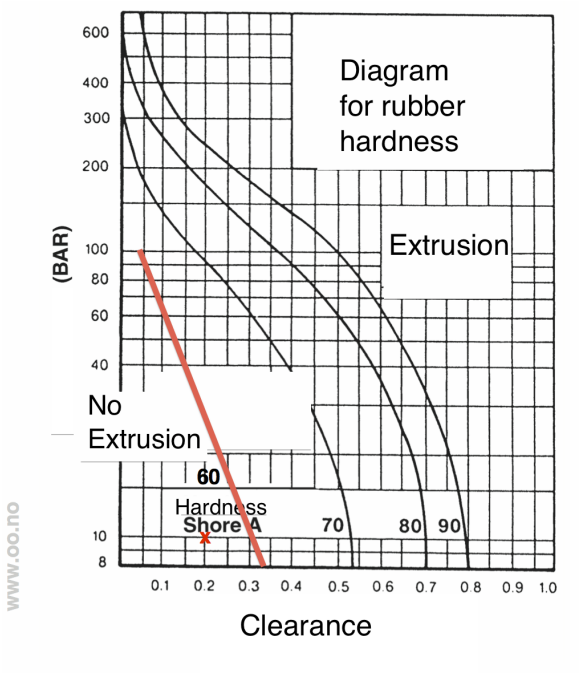

FIGURE 7.3: This graph shows the behavior of extrusion in o-rings as a function of gap and pressure. The red line describes the anticipated graph for Shore 60 hardness and the red x where the chosen design is. Adapted from [26]

Mould tooling

By using the principles described in the previous section the tool shown in Figure 7.4 was constructed. The dimensions of the platen press and the stakeholders laminate thickness requirements were natural constraints to the dimensions of the tool. Machine drawings are attached in Appendix E . The test setup should seek to mimic a general aerospace skin part. Thus a generic geometry should be used.

[1] Shore A hardness is a measurement of the hardness of the material. The measurements is done by indenting a cone in to it and by observing the size of the mark indented.

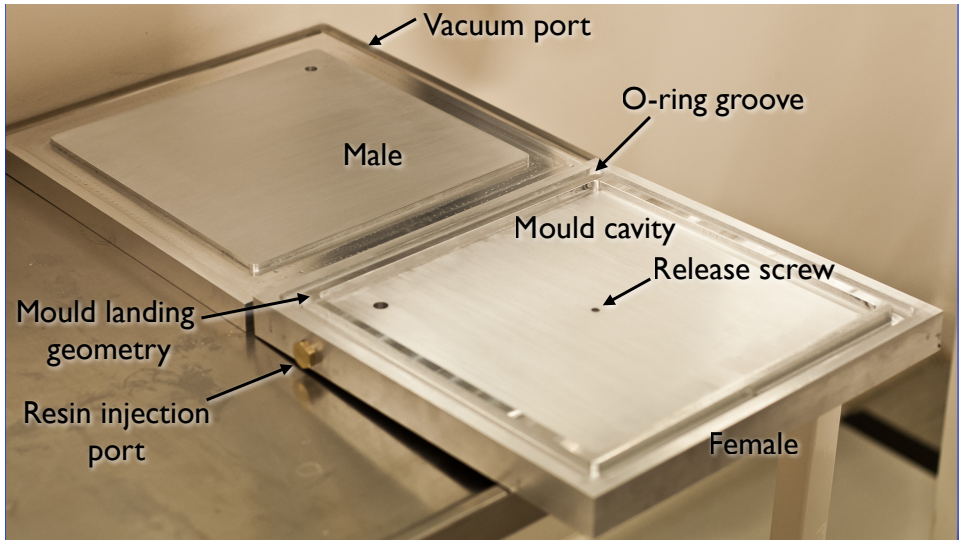

FIGURE 7.4: The mould tooling fabricated during the project work [27].

In order to grasp a large area of parts, both a flat plate tool and a sandwich plate tool was fabricated. The sandwich plate tool was designed to use the same upper tool half as the flat plate tool. The lower part of the sandwich tool can be seen in Figure 7.5.

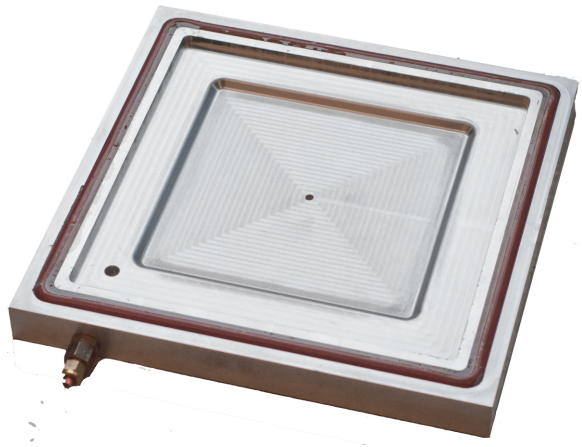

FIGURE 7.5: The sandwich plate tool and O-ring can be seen in the figure. The cavity for the core is the difference from the flat plate tool.

Resin flow

Vents and injection ports are categorized as radial or axial. To favor large resin flow an axial resin injection port is beneficial. This is because the pressurized resin is able to contact a large fibre area in the preform periphery. All though it is beneficial it contradicts the net shape moulding technique as the periphery should be un obstructed to avoid circumferential machining. Also, the flow path can be shorter for a center mounted radial inlet than for a periphery mounted axial inlet. Due to the importance of net shaped parts in this application radial inlets are chosen both for resin injection and vacuum outlet. For large aerospace skins multiple injection ports will be necessary because the extent of the part is longer than the possible resin flow. In these situations radial resin injection is impossible to avoid.

Due to the fact that a platen press should be used no obstructions could be present on the top or bottom surface of the tool. This led to a more advanced sprue geometry than strictly necessary. The internal design of the mould tool is depicted in Figure 7.6. An evident challenge with sprue design is the curing of the resin inside the sprue. This has to be removed before the tool can be reused and can be seen in Figure 7.7. The sprue has to be designed so this can be done easily.

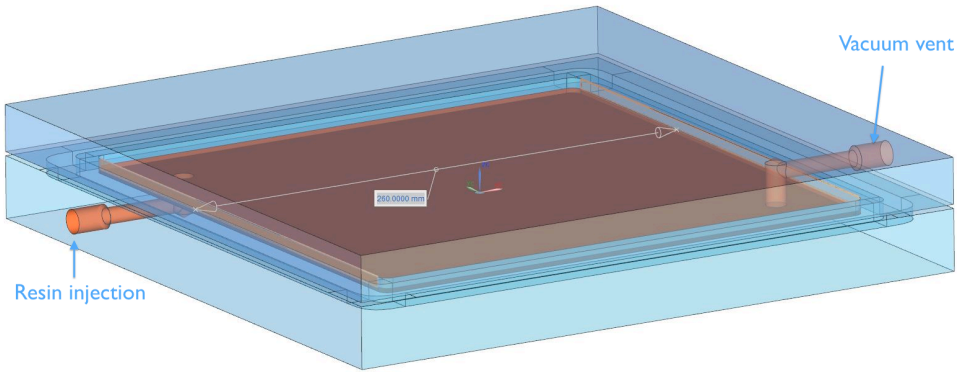

FIGURE 7.6: 3D model of the mould cavity with sprue (resin injection) and vent. The gates have to enter the tool from the sides because of the constraints from the platen press.

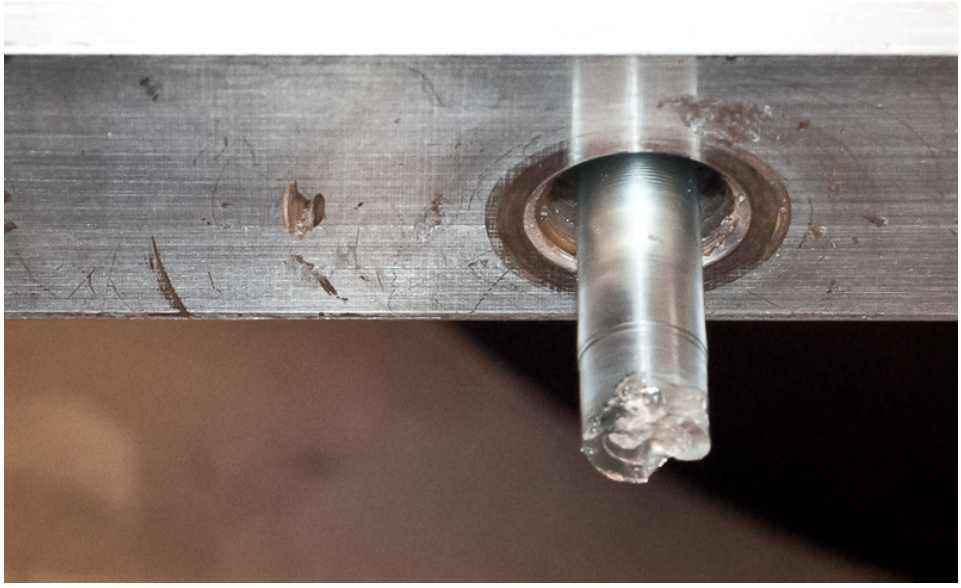

FIGURE 7.7: The picture shows resin cured in the tool sprue.

Mould cavity

The mould cavity was set to be approximately 2.2 mm thick and 260 mm × 260 mm in in pane dimensions. Corners were given a radius of r = 5 mm, this measurement constrains the size of milling tool possible to use while machining the mould. Hence, this is a large cost driver, as a halving of the mill size will roughly double the machining time of the cavity. For the transition from mould surface to vertical flange no radius was specified. Thus, it will be very small and given by the end mill used. If this radius can be small in terms of demoulding it will strengthen the net shape method as sharp corners often are desired.
There are different ways of implementing the parting plane in the tool. In consideration of different solutions the ease of fibre debulking and demoulding should be evaluated.

For Figure 7.8a) and 7.8c) the debulking of the fibre preform might be difficult. After the preform is placed in the mould it will be debulked by the closing action of the tool. If the preform exceeds the boundaries of the bottom tool half it can expand outwards during the closing and get stuck between the two mould halves.

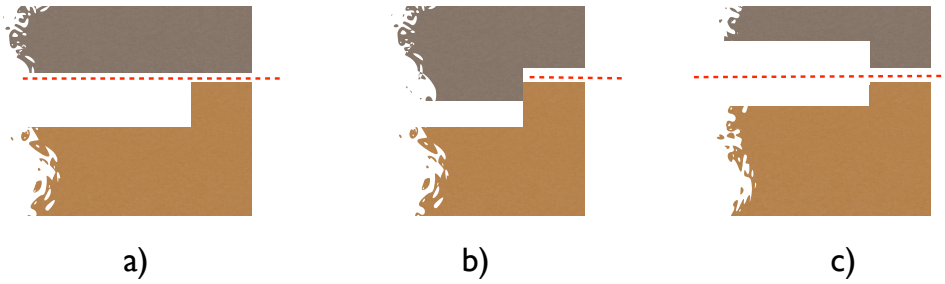

FIGURE 7.8: Three different ways of implementing the parting plan in the tool. The dotted red line indicates the parting plan.

If the tool is closed in this manner it will destroy the tool. Further there has to be a sealing geometry outside the landing geometry so the stuck fibre will be almost impossible to predict. The method in Figure 7.8b) is therefore the method of choice. Additionally, this way of doing it provides a self aligning geometry that ensures the tool always to be properly closed. For the other possibilities an alignment geometry would have to be added separately.

7.2 Resin Injection

Resin needs to be injected in to the tool in a controlled way. Off-shelf solutions are available but the price of such devices is high [28]. An investment like this was not feasible in this work, therefore an in house mechanism was design and fabricated for this purpose. As seen in Chapter 4 a resin pressure exceeding 7 bar does not yield noticeably lower void content in the laminate. The fact that the workshop floor pressurized air obtained a pressure of 7.2 bar was gladly welcomed. Consequently a solution utilizing this pressurized air was designed. Figure 7.9 shows a principle sketch of the chosen concept.

The viscosity of the resin depends heavily on the temperature. E.g. for the injection resin used the rehology is described in Figure 5.6. From this it is evident that some sort of temperature control for the resin injection is necessary. The pressure vessel described earlier was therefore placed in an oven in order to heat the resin.

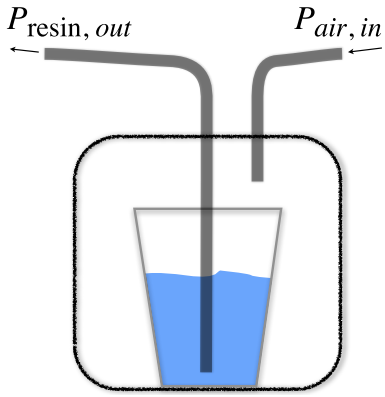

FIGURE 7.9: Principle sketch of the concept for resin injection. The blue area resembles resin and the black boundary a pressure vessel.

The finished setup can be seen in Figure 7.10.

(A) The resin pressure pot in side an oven as it was used in the experiments.

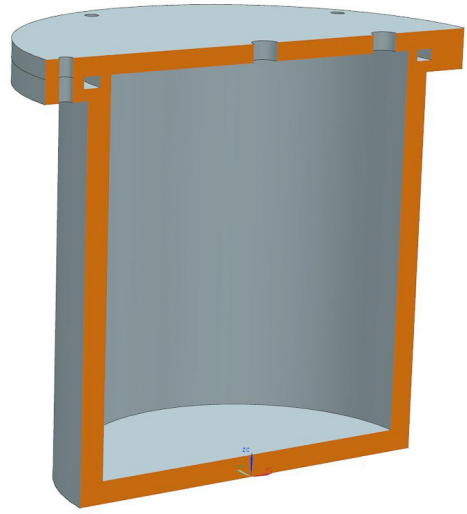

(B) 3D illustrasion of the pressure pot.

FIGURE 7.10:

7.3 Miscellaneous components

The mould tool and resin injection system is the main constituents in the SQRTM-setup. In order to connect the two subsystems some sort of hose and fitting system should be used. Due to the high curing temperature of the 6376-resin the whole system needs to withstand at least 175 °C. Copper tubing was chosen and used to connect all the subsystems. Copper fittings were used and inserted in to threaded holes of the different components. The valves were fitted accordingly. As a consequence of the resin flow through the system all components where resin had been present either had to be cleaned or replaced. All tubing between the pressure pot and the exit valve (including the valve it self) had to be replaced for each curing cycle. In commercial available systems cleaning of the tubes is possible to achieve automatically before the resin gels. Thus yielding less disposals. Fittings that contained cured resin were drilled open for reuse. Apart from the system it self an oven was needed for the hot debulk process. The system is depicted in Figure 7.11.

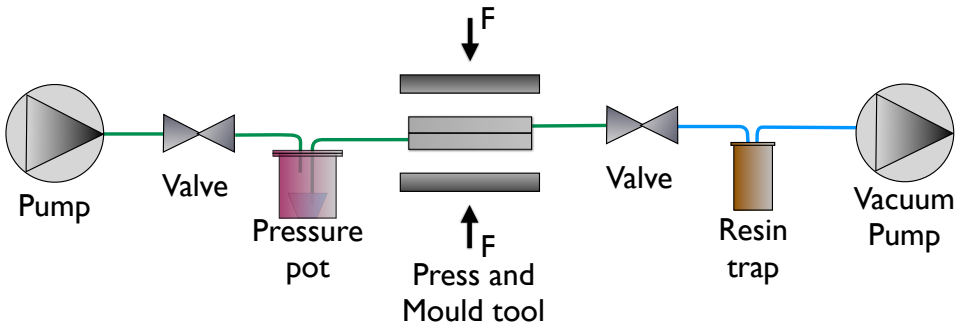

FIGURE 7.11: The figure illustrates the SQRTM-system used in the experiments. The green tube resembles copper tubing and the blue tube resembles plastic tubing.

Chapter 8

Experiments

During the working period of this thesis a number of four flat plates and two sandwich plates have been moulded. In addition a three point bending test has been executed on the flat plates. In order to evaluate the results of the experiments a good laminate was defined as the following:

Low void content: No visible voids at 100× magnification.

Good surface finish: No visible surface flaws.

High flexural strength: Flexural strength comparable to autoclave laminate or higher.

8.1 Flat plate moulding

In Chapter 6 the authors understanding of the SQRTM method is presented. This approach was implemented in the experiment. From earlier work [27] debulking had proven useful. Also it was evident that hydrostatic resin pressure was important in order to obtain a good surface finish. The experiment sought to understand the important of hydrostatic resin pressure and the effects of preform debulking.

Four plates were made with two different materials. The materials are designated material A[1] and B[2]. The tests are named with a T for the ones made in the thesis work and a P for the ones made in the project work.

TABLE 8.1: Tabular representation of the experiments conducted.

Test	External resin pressure	Dwell at 175 °C	Applied vacuum	Debulk	Layup	Material
T1	N/A	2 h	N/A	10 min per ply* + 10 min @ 60 °C	8 plies	A
T2	N/A	2 h	Yes + vac. closing	5 min per ply + 10 min @ 60 °C	8 plies	A
T3	7 bar	2 h	Yes	5 min per ply + 10 min @ 60 °C	8 plies	A
T4	7 bar	1 h	Yes	10 min per ply	4 plies	B

*The stack with six plies were left under vacuum for 60 min.

All the four preforms were debulked thoroughly. A vacuum bag was applied subsecuently between each ply during the preform building. The debulk layup can bee seen in Figure 8.1. This was done in room temperature. For the hot debulk indicated in Table 9.1 the preform with vacuum bag was placed in an oven. The thermal contraction of the tool has previously been measured to be 0.78 mm. This yields a normal stress in the laminate of 218.5 MPa and a flange shear stress of 70.3 MPa. The calculations can be seen in Appendix C. None of these values are critical. Cold demoulding is therefore viable.

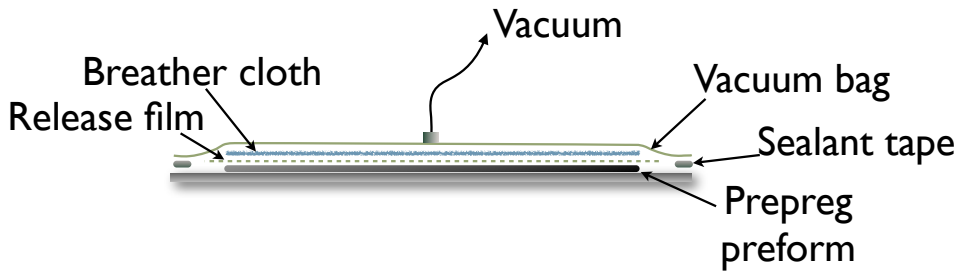

FIGURE 8.1: Illustration of the debulk lay up sequence. Peel ply can be fitted between the release film and breather plies. This was found redundant if the breather was rigid enough.

[1]HexPly® 6376C-905-36%
[2]ACG LTM®16

General procedure:

First, and before the debulked preform was placed in the mould cavity, resin was placed in the heated pressure pot and drawn to the tool in order to evacuate the air in the tube. The resin pressure was not elevated until later. The preform was now placed in the mould cavity and the mould closed with a high force (usually 210 kN). The desired temperature was dialed in to the control system and the temperature raised. Simultaneously vacuum was added through the venting port, following that, the resin pressure was raised to the desired injection pressure. The vacuum was held until resin was flowing out of the vent. The resin pressure was held throughout the entire curing cycle.

T1. This test was carried out in order to isolate the effect of preform debulking. Hence, no resin was injected. The preform was thoroughly debulked and placed in the mould cavity. Inlets and outlets were blocked with pre-cured resin. The mould was heated to 175 °C and cured at dwell temperature for 2 hours.

T2. To avoid enclosing of air in the cavity upon tool closing a test with vacuum closing of the tool was performed. First the preform was built directly on to the female tool half and subsequently debulked as previouly described. This ensured no air on the lower surface of the laminate. Guiding-holes were machined in the mould tools and guiding-pins inserted in order to allow for a controlled large gap closing. Cork spacers were placed in between the mould halves to generate distance between the mould halves. Afterwards the tool was bagged along the circumference and a vacuum was drawn through the vacuum vent of the tool. When vacuum pressure was obtained the tool was closed by the platen press. This compressed the cork spacers to a very flat state. The vacuum vent was closed after the tool was closed. The assembly of the system is depicted in Figure 8.2.

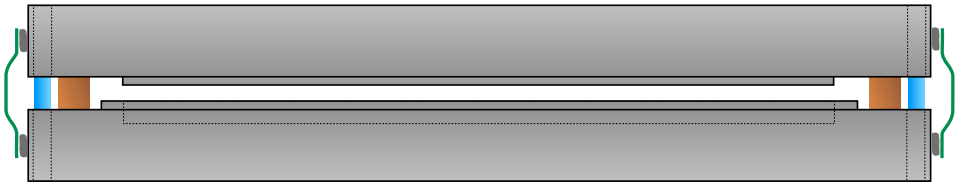

FIGURE 8.2: The figure shows a 2D illustration of the mould tool with a circumferential vacuum bag (green), guiding-pins (blue) and cork spacers (brown) as used in test T2.

T3. It was evident that the injection resin[3] posed certain challenges to the setup as the rehology of material A and the injection resin was widely different[4]. To overcome this difference the injection resin was injected with no hardener. This would facilitate low resin viscosity throughout the cure of the prepreg. However, the laminate would not be structurally sound. Apart from that the general approach was followed. For this test holes were drilled in to the mould tool in order to insert thermo couples. The temperature was thus logged throughout the curing cycle both in the upper and lower tool half.

T4. Due to the mismatch between the injection resin and material A this test was executed with material B and the injection resin. The general approach was followed but the curing cycle was adjusted to fit the new material. The imposed curing cycle can be seen in Figure 8.3. Unfortunately, the rehology of material B was not possible to find in the literature. Therefor, the ramp up procedure was done iteratively in order to facilitate low resin viscosity and high resin flow. A low temperature curing cycle was recommended for this material. Therefore it was likely to suite the injection resin better. The vacuum vent was shut when the resin was observed flowing through the vent.

[3]EPIKOTE Resin MGS® RIMR 135 [29]

[4]The injection resin was a room temperature curing system and material A was cured at 175 °C

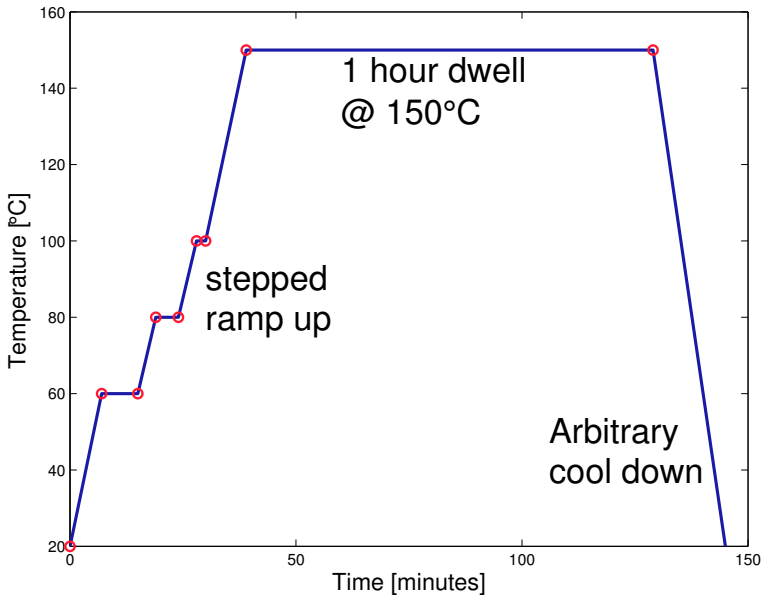

FIGURE 8.3: The graph shows the temperature readings (red circles) from the platen press during the cure cycle.

8.2 Sandwich construction moulding

In addition to flat plates, tests of the SQRTM method were run with sandwich plates. A separate lower tooling half was machined to allow for a 5 mm thick core[5] section (See Figure 8.4). The tests were run according to the *general procedure* in Section 8.1. Here the lower carbon fibre skin was debulked directly on to the lower tooling half and the upper skin was debulked separately on a flat plate. Both skins were subsequently debulked for 5 minutes per ply. Normal practice in Rohacell prepreg consolidation in matched moulds is to oversize the foam core so it can act a positive pressure on the prepreg [23]. This helps to raise the hydrostatic resin pressure. In this experiment however, the cores were machined net size as the injected resin should elevate the resin pressure.

Test Tc1 was run without external resin pressure in order to obtain a lower bound reference sample. For test Tc2 material B was chosen as it was more applicable with

[5]ROHACELL® 110 WF-HT. A closed cell foam material made from BMI.

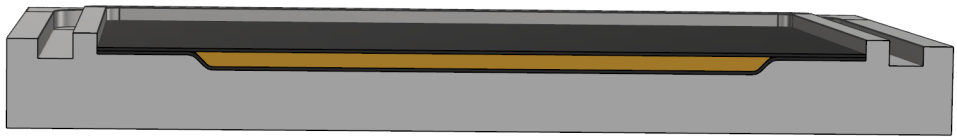

FIGURE 8.4: 3D sketch of the lower tooling half with slot for core material. The upper and lower carbon fibre skin is here placed. The core is in between.

TABLE 8.2: Tabular representation of tests executed with sandwich plates.

Test	External resin pressure	Dwell at 175 °C	Applied vacuum	Debulk	Layup	Material
Tc1	N/A	2 h	Yes	5 min per ply	4 plies core 4 plies	A
Tc2	7 bar	2 h	Yes	5 min per ply	2 plies core 2 plies	B

the injection resin. Tc2 was run according to the *general procedure* in Section 8.1. A stepped ramp up, corresponding to Figure 8.3, was used. This was the chosen ramp up for both tests with material B.

8.3 Miscellaneous injection tests

In addition to the tests with preform filled cavity two tests were executed with no fibre preform. Previous work [27] showed that bubbles were present on the surface of the laminate. Seeking to understand the origin of these bubbles the following two tests were run.

Empty cavity resin injection

Neat epoxy resin was injected in to the empty cavity. A steady flow of epoxy through the vacuum vent was obtained before the vent was closed. Resin pressure was obtained throughout the cure.

Breather cloth resin injection

A stack of four plies of breather cloth was placed inside the cavity. Epoxy

resin was injected and the vacuum vent was closed when the resin flowed out of the vent. The resin pressure was obtained throughout the cure.

8.4 Three point bend test

In order to evaluate the different test laminates a three point bending test was performed. This testing method is best suited to compare different laminates qualitatively. Better laminates yields higher values of short beam strength. This value can be interpreted as for instance ILSS if the failure mode is consistent. This is done in the paper by Davies et al. [17]. Here the resin from material A was used with a unidirectional fibre reinforcement. Inspired by the paper the ASTM D2344M [18] standard was chosen. A three point bending rig was built according to the specifications (as in Figure 8.5b). The test specimens were cut on a diamond bladed saw. The standard indicates that the specimen dimensions shall relate to the laminate thickness as shown in Figure 8.5a.

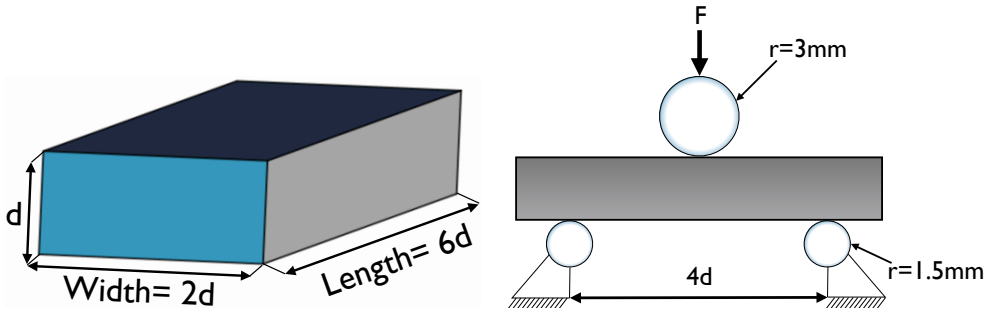

(A) (B)

FIGURE 8.5: The Figure shows the dimensions of the specimens and the three pint bending rig as per ref [18].

The crosshead velocity was set to 1mm/min. A total of 20 specimens from five different plates were tested. All fabricated from material A. The specimens were taken from test P1, P5, T1, T2 and T3. P1 and P5 were included for reference to the older tests. This made it possible to better understand the functionality of the

debulk and resin injection. The tests were conducted on an Instron hydraulic test machine.

Three point bending modeling

A FEA model of the three point bending test was established in the ABAQUS software. The linear elastic simulation was carried out in order to investigate the failure mode of the three point bending test. Assuming that if the FEA results fit the experimental results a nearly linear elastic shear mode was the mode of fracture in the test. Due to symmetry in the setup only half of the system was modeled. The meshed parts can be seen in Figure 8.6 The simulation was run after

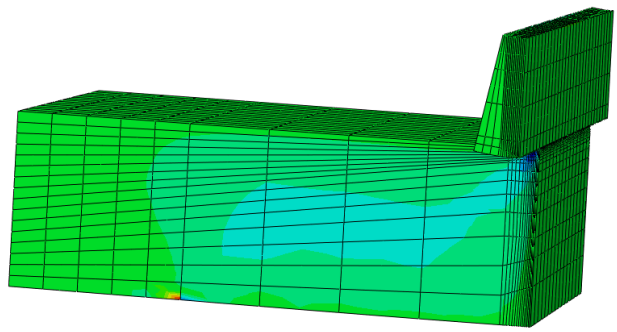

FIGURE 8.6: The deformed system with a S13 superimposed plot can be seen in the figure.

the physical experiment. In order to compare the two, the maximum load exerted in the experiment was applied in the FEA model. Material properties were assigned to a homogenous section with the following engineering constants:

TABLE 8.3: Engineering constants used in the FEA model*

E_1, E_2	E_3	$\nu_{12}, \nu_{13}, \nu_{23}$	G_{12}	G_{13}, G_{23}
67000	10000	0.08	2840	2000

* MPa (except for ν_{ij})

As a consequence of the load case, the model was meshed with *C3D20R* elements. These quadratic brick elements exert bending stiffness [30] (as opposed to linear

elements) and are therefore suitable for the shear load in this model. Symmetry considerations were implemented in the symmetry plane as seen in Figure 8.7 alongside with the other constraints and loads. The load was applied through a reference point that was tied to the upper surface of the cross head. The cross head was modeled as steel. Hard contact constraints were applied between the laminate specimen and the load bar. Friction was neglected.

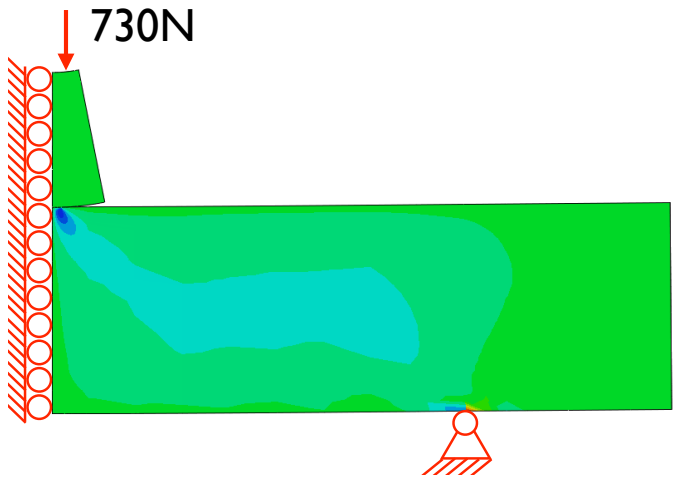

FIGURE 8.7: The constraints and loads applied to the model is shown.

From the experiment a load of 1460 N was found to be the maximum load before failure. Half of this load was applied to the load bar as only half of the model was present. The different normal stresses were checked as an indication that both the load and the material properties were approximately correct. Plots of S11 and S33 are shown in Figure 8.8.

The stresses on the laminate is within sound values as the technical data sheet [7] states that tensile strength is $X_T = 1006\,\text{MPa}$ and compression strength is $X_C = 920\,\text{MPa}$. The compression in 3-direction is dominated by the resin properties. The technical data sheet for the resin gives a tensile strength value of 105 MPa. However, the large compression values in the test are located near the supports and beneath the load bar. Here singularities are present and as a consequence these values are omitted. In the real experiment the load bar vill contact a larger area

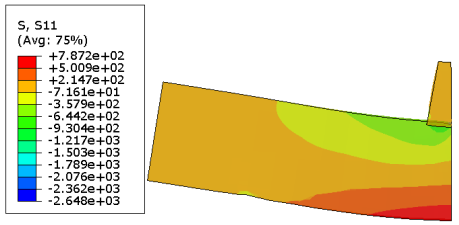

(A) Stress in 1-direction is shown. Maximum compression is about 650 MPa and maximum tension 790 MPa. 20×deflection

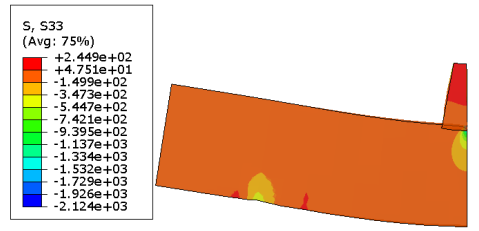

(B) Stress in 3-direction is shown. Most of the laminate is in a very low state of compression. 20×deflection

FIGURE 8.8:

due to yielding of the material and the concentration of loads around the supports will be lowered. This effect is not seen in the linear elastic model depicted.

The inter laminar shear component of interest is S13. This is ploted for different distances from the plane of symmetry in Figure 8.9 The results coincide well with the experiments as both the experiment and the simulations give approximately the same values for the maximum interlaminar shear stress when the same load is applied. Although the values of S13 near the symmetry plane is very high, that is. These values are neglected due to the bad load transmission between the load bar and the laminate. The deflection at the load bar was found to be 0.032 mm in 3-direction. When a specimen is loaded in this manner both large shear and normal stresses occur. The ratio of maximum shear stress to maximum normal stress was calculated with beam theory and found to be:

$$\frac{\tau_{\max}}{\sigma_{\max}} = \frac{1}{2}\frac{d}{L} = \frac{1}{8} \tag{8.1}$$

Where d is the specimen hight and L the length between the supports. The calculations can be seen in Appendix B. As the X_T yields the stress of failure the in normal stress the flexural strength of the resin is important for the shear failure. The flexural strength of the resin is 144 MPa per the technical data sheet [31]. In this test the shear strength value should be reached first. $\frac{1}{8} \cdot X_C = 115$ MPa. Implying that, if the short beam strength values obtained are lower than 115 MPa

the failure mode vill most likely be shear as the compressive strength is not yet challenged.

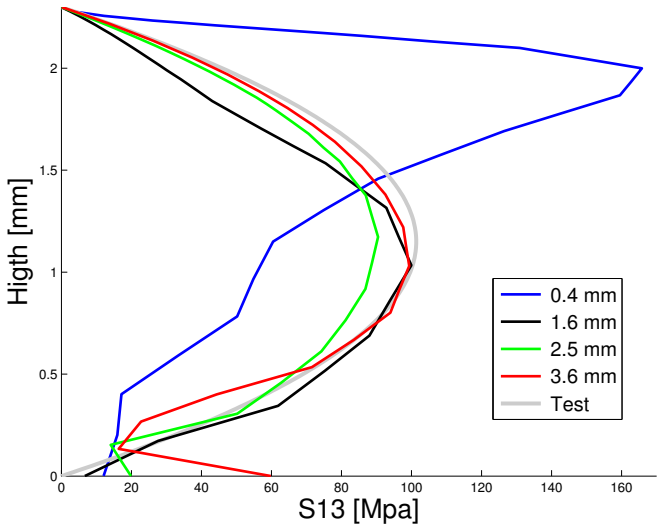

FIGURE 8.9: The Interlaminar shear stress (S13) is plotted through thickness at a given distance from the symmetry plane. The assumed distribution experienced in the test bears the legend *Test*.

Chapter 9

Experimental results

9.1 Flat plate moulding

Four different flat plates with prepreg preform have been moulded in the work with this thesis.

T1

Very bad surface finish. White dots are present on the entire lower surface. The upper surface contains large good areas, but some pinholes are present here as well. Voids can easily been seen in the microscopy picture (Figure 9.1c)

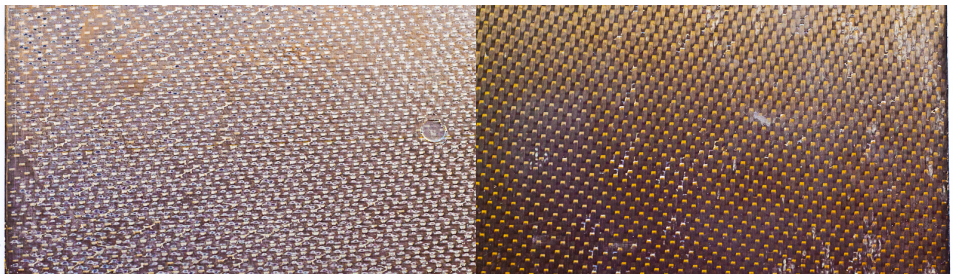

(A) T1 - Bottom (B) T1 - Top

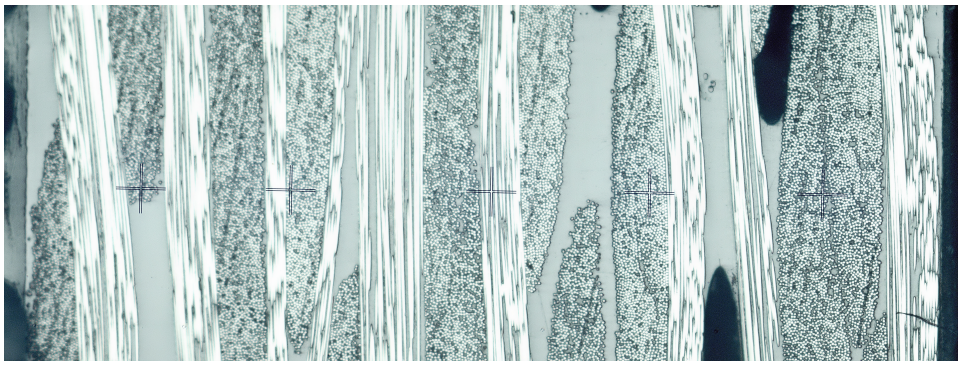

(C) T1 - microscopy cross section

FIGURE 9.1

T2

Somewhat better surface finish than T1, but the plate still contains some white dots and pinholes/ holes in the surface. During the execution of the test no resin flowed through the vacuum vent. Both intralaminar and interlaminar voids can be seen in the microscopy picture below.

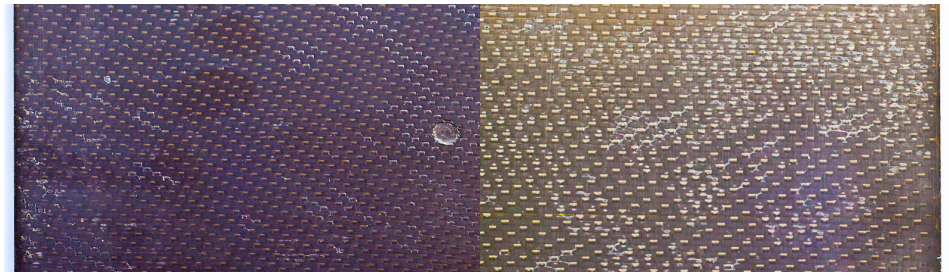

(A) T2 - Bottom (B) T2 - Top

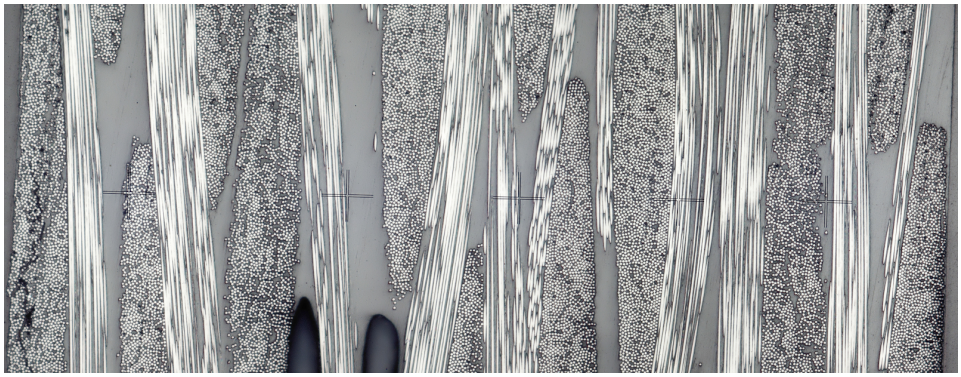

(C) T2 - microscopy cross section

FIGURE 9.2

T3

Large perfect areas observed on the surface. These contains no pinholes or other flaws. Large areas are dry and fabric looking. The temperature measurements done during this test can be seen in Figure 9.4. All tests with material A were run with this curing procedure. The microscopy picture shows no interlaminar voids. Some small black dots are present. This can be small intralaminar voids or just residuals from the polishing of the specimens.

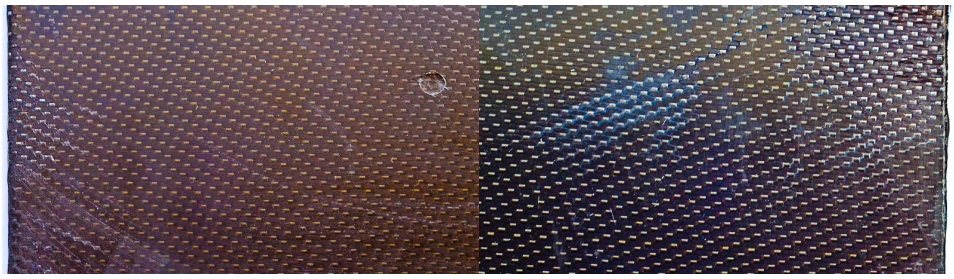

(A) T3 - Bottom (B) T3 - Top

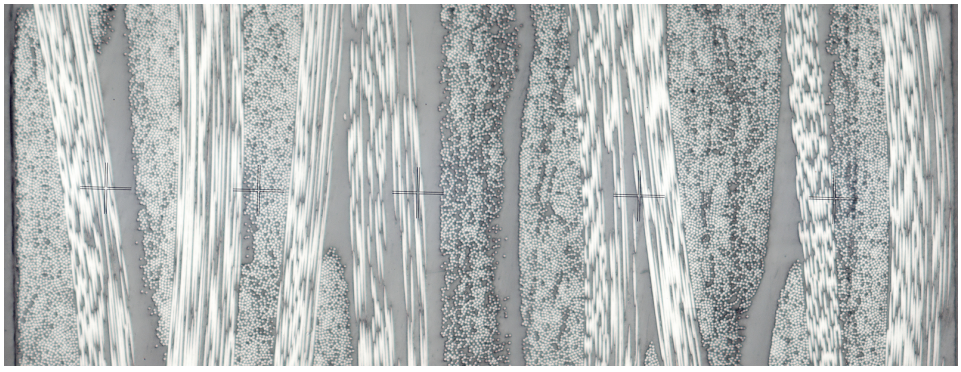

(C) T3- microscopy cross section

FIGURE 9.3

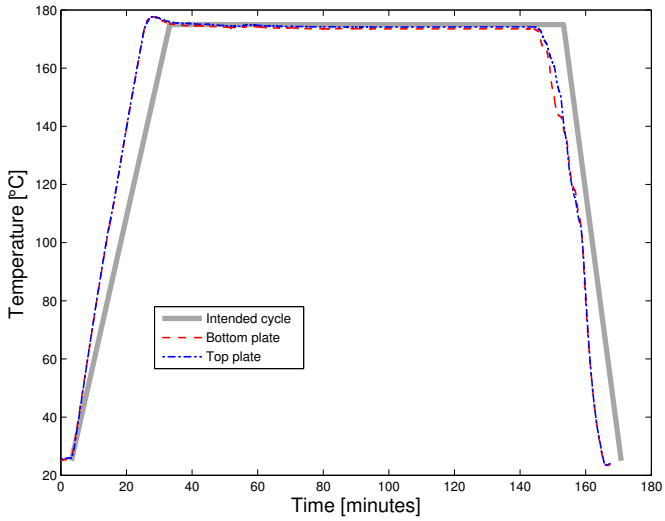

FIGURE 9.4: The plot show the measured temperature progress in the mould during test T3.

T4

The surface finish is very good. No fault or pinholes are visible on the surface. The surface is homogeneously good with no bad areas. This material was apparently a better mach for the injection resin than what material A was as resin was able to flow out of the vacuum vent. The microscopy shows no large voids. The black lines look like residuals from the polishing or even bad sample preparation. Tiny intralaminar voids are present.

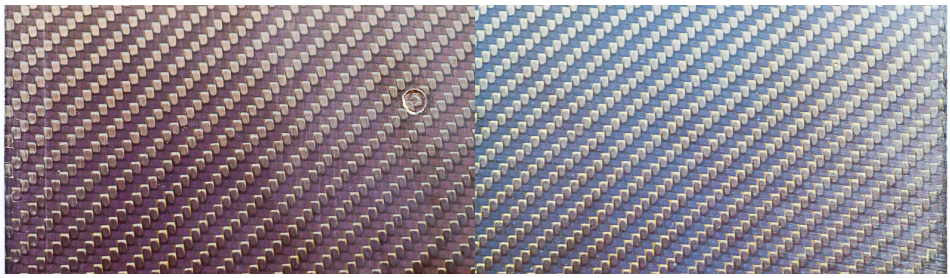

(A) T4 - Bottom (B) T4 - Top

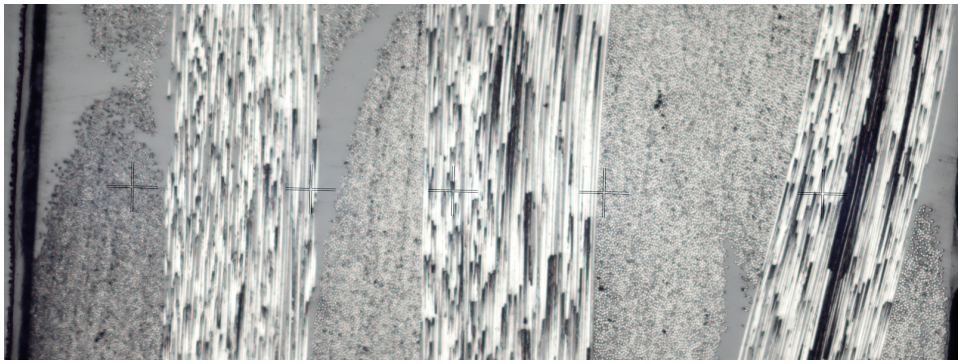

(C) T4 - microscopy cross section

FIGURE 9.5

9.2 Sandwich plate results

Tc1

The surface quality is quite good. There are no white dots on the surface, but some pinholes and dry spots are present. Dry spots are especially salient in the corners of the core material and the inclined part on the surcsumfereance of the core.

Tc2

Good and smooth surface finish. No dry areas observed, but some pinholes are present. The circumference of the core prints through the upper skin.

(A) Cross section of Tc2, the foam is the core material which adequately fills the gap between the lower and upper skin.

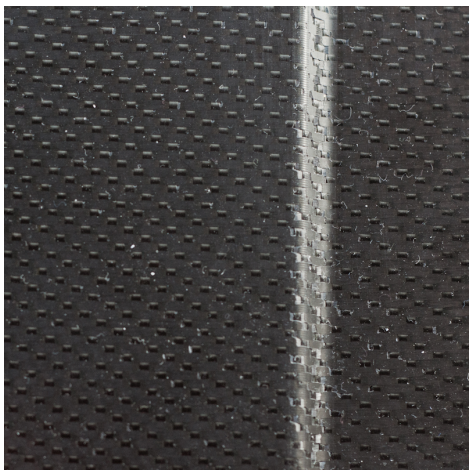

(B) The transition to the core material in Tc1. Surface flaws can bee seen.

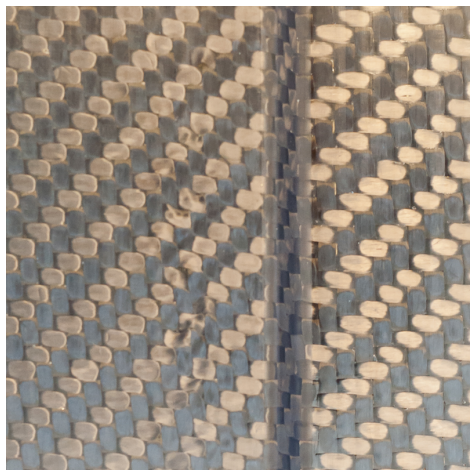

(C) The transition to the core material in Tc2. No visible surface flaws.

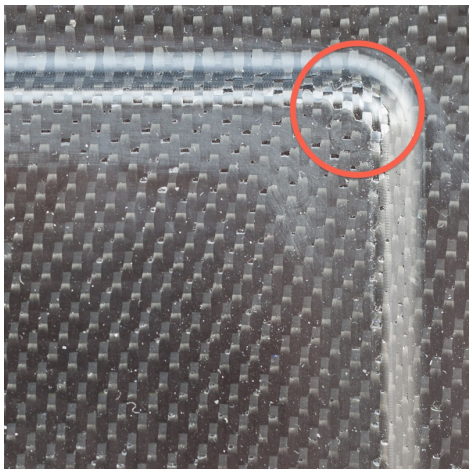

(D) Corner of the core material, Tc1. Dry areas are outlined in red.

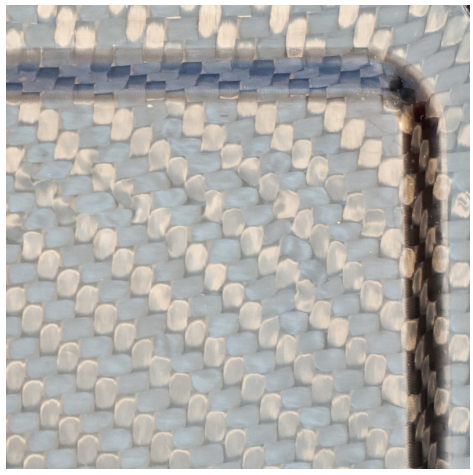

(E) Corner of the core material, Tc2. No dry areas present.

FIGURE 9.6: The pictures shows different sections of the sandwich plates moulded.

9.3 Miscellaneous injection test results

Both tests gave plates with shape according to the mould cavity that filled the cavity well. No dry-spots were found in the breather cloth plate. By the naked eye the leaf shaped bubbles outlined in Figure 9.7 were almost invisible. Some circular bubbles were entrapped in the resin. All of these were located at the corners of the plate where the gates are not present. In the breather injection plate a re die was mixed in the resin. However, this was not visible when tried out in a prepreg preform.

9.4 Three point bending results

The three point bending test was conducted as previously described. The results obtained was treated according to ASTM D2344M [18]. In addition a characteristic value was obtained. The load and displacement of the cross head was continuously measured. The maximum reading of the force from each test was divided by the specimen cross section area as per Eq. (9.1).

$$F^{sbs} = 0.75 \times \frac{P_m}{b \times h} \tag{9.1}$$

According to [18] this gives the short-beam strength (F^{sbs}), where P_m is the maximum load, b is the specimen width and h the specimen thickness. The means ($\bar{x}$) and sample standard deviations (S_{n-1}) were then found by applying the following equations,

$$\begin{aligned} \mu = \bar{x} &= \left(\sum_{i=1}^{n} x_i \right) / n \\ \sigma = S_{n-1} &= \sqrt{\left(\sum_{i=1}^{n} x_i^2 - n(\bar{x})^2 \right) / (n-1)} \end{aligned} \tag{9.2}$$

by assuming normal distribution of the test data. The standard normal distribution gives,

$$1 - \mathrm{P}(Z < -2) = 1 - 0.0228 = 0.9772 \tag{9.3}$$

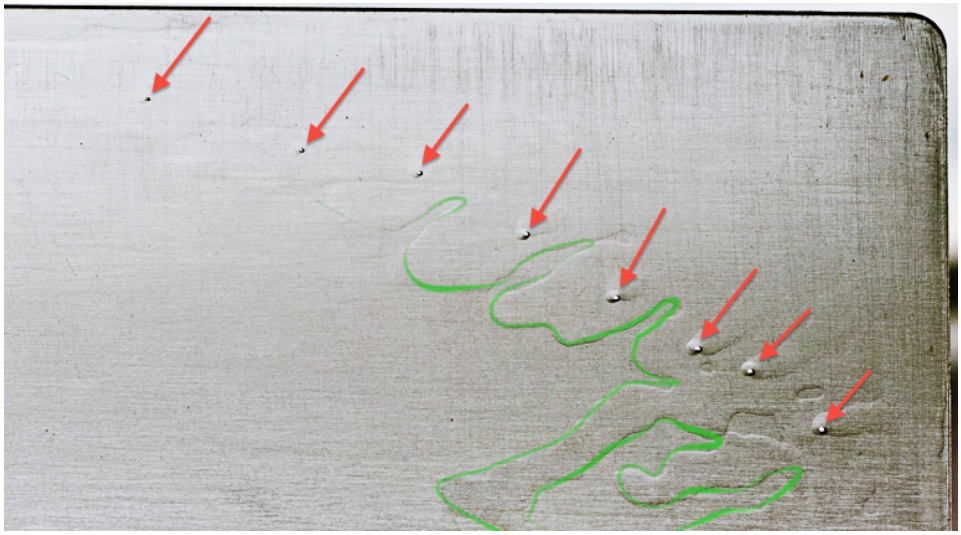

(A) Empty cavity resin injection

(B) Breather clot resin injection

FIGURE 9.7: The high contrast images shows the plates from the test. Leaf shaped bubbles are outlined in green and small visible spherical bubbles are indicated by red arrows.

meaning that 97.7% of all tests lies beyond a $\mu - 2\sigma$ lower bound as the standard deviation is one for the standard normal distribution. The results obtained are described in Table 9.1,

Additionally a cross section normalized load (named short beam shear) was plotted for the entire progress of the test. These results were plotted as in Figure 9.8. The

TABLE 9.1: Three point bending test results*

Test	μ	μ_{norm}	σ	$\mu - 2\sigma$	Failure mode
T1	96.2	101.4	5.4	85.4	Flexure – Compression
T2	91.2	95.3	2.7	85.8	Flexure – Compression
T3	89.2	94.4	4.3	80.6	Interlaminar shear
P1	72.3	79.6	3.6	65.2	Flexure – Compression
P5	86.7	91.4	3.7	79.4	Interlaminar shear

* μ is avarage Short beam strength in MPa.
μ_{norm} is avarage Short beam strength normalized for 60.2%v_f.
σ is standard deviation.
$\mu - 2\sigma$ is characteristic value for each test.

maximum points indicated in the plot coincides with the short beam strength. A $\pm 2\sigma$ error-bar is plotted with the average point. The plots for the accompanying tests can be seen in Appendix B. Short beam shear was calculated per Equation 9.4.

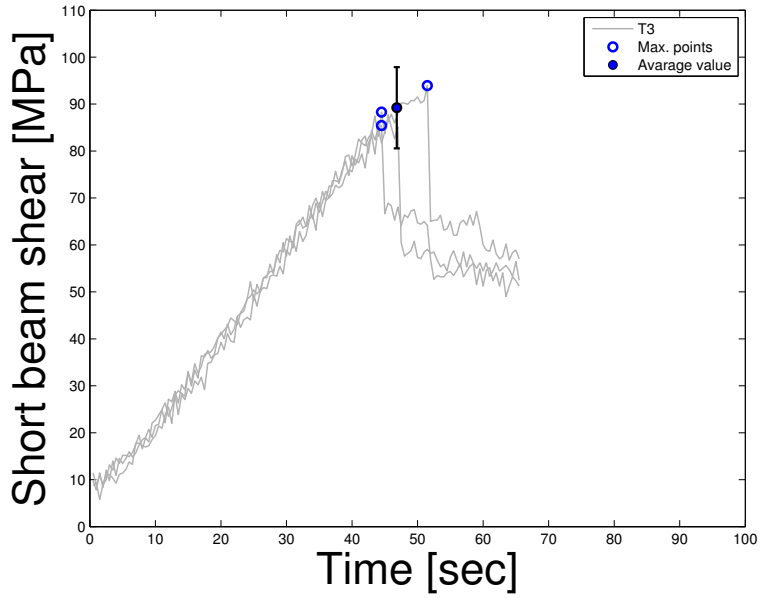

FIGURE 9.8: The figure shows a Short beam shear – Time plot for the different samples from test T3.

$$F^{sbr} = 0.75 \times \frac{P}{b \times h} \tag{9.4}$$

Where P is the continuously measured load and F^{sbr} the short beam shear. Some problems were encountered with the test machine during this test. After the tests

were run i was obvious that the displacement readings were wrong. Consequently they are not included in the plots. However, the displacement is not important in the short beam shear test.

Chapter 10

Discussion

The superior quest of this work is to understand how high quality laminates can be obtained with the SQRTM method. Thus, the Discussion chapter revolves around the question: *what makes a laminate good with the SQRTM – technique?* The three criterions – *low void content, good surface finish* and *high flexural strength* are discussed to answer this question.

10.1 Flexural strength

The normalized short beam strength values show differences between the various tests. This is Shown in Figure 10.1a. The characteristic values shows that T1 and T2 performs equally in the three point bending test. T3 is better than P2. On the contrary, P1 is by far the weakest result. All tests but P1 were vacuum debulked. P2 is debulked less than T1, T2 and T3. Consequently this might indicate that vacuum debulking is beneficial for short beam strength. Other properties that possibly can affect the short beam strength is surface finish. However, the test with the least good surface finish yields the highest short beam strength. This possibility is therefore ruled out. It is known that fibre volume fraction greatly

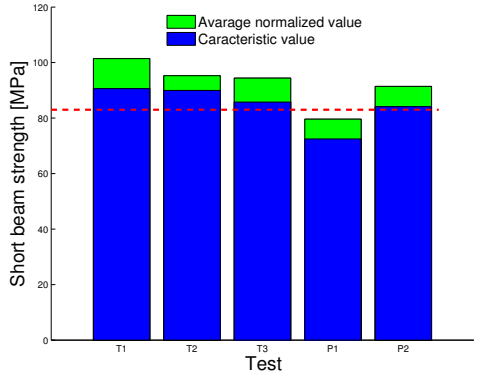

(A) Graphical illustration of the 3 point bending test results normalized for 60.2% fibre volume fraction.

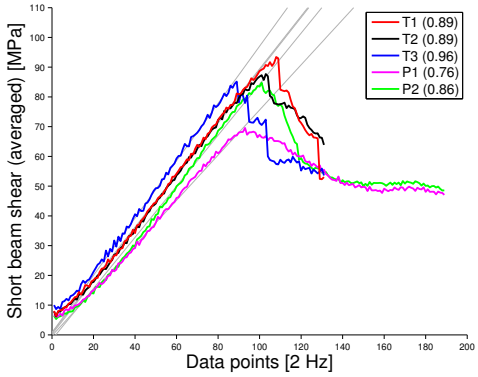

(B) The graph shows averaged short beam shear for the different tests. The linear part of each curve is ploted in gray. The slopes of these are given in the brackets.

FIGURE 10.1

affects the results. Hence, the results are normalized to provide comparable results. The trends in the data set are not changed by this. It is therefore suggested that the discrepancy in fibre volume fraction is not so large that the results are severely influenced. The stiffness[1] of the specimens is given by the slope of the curves in Figure 10.1b. Resin injection was performed on T3 and P2 only. It is seen that T3 is the most stiff specimen. Similarly T1 and T2, that were given the same debulk and similar consolidation procedure, yield the same stiffness. P2 was less debulked than T3, T2 and T1. The stiffness of P2 is, in that regard supposedly, lower than all of these specimens. P1, that was not injected with resin, nor debulked yields the significantly lower stiffness. For the reasons presented it is suggested that resin injection and debukling is favorable for the bending stiffness of the laminate. The latter more important. The same inference is proposed for the short beam strength. The failure of each specimen is characterized by the slope of the curve that exceeds the maximum point (the point of failure). The most significant difference is here between P1 and the other specimens. This difference can be interpreted in the following way. A good laminate can withstand a high amount of strain energy before failure. When failure occurs in small parts of the cross section the residual

[1] In a short beam shear – strain plot this is proportional to the flexural modulus of the laminate.

strain energy is distributed over the remaining cross section. A higher initial strain energy equals a higher residual strain energy. The remaining cross section continues to fail if the residual strain energy is too high, thus yielding a steep falling slope from the point of failure. By applying this deduction it is understood that the properties of a material is obtained in a best possible way if the specimen shows a steep falling slope. Consequently, P1 is not exploiting the potential of the material system as it brakes gradually. The effects of resin pressure and debulking is therefore believed to be crucial to obtain a laminate with high flexural strength. The autoclave results is shown in the technical data sheet [7] and reads 83 MPa. As depicted in Figure **??** the normalized characteristic values exceeds this limit. Except for P1 that is. For this reason the flexural strength of the laminates are considered to be good. The paper by Davies et al. [17] was a great inspiration in this testing method. The 6376-resin was used here as well and the data were normalized for 60.2 % fibre volume fraction. For this reason the values in Figure 10.1a were normalized accordingly. The total mean value of all tests in the paper is ILSS=97.6 MPa. This includes a variety of curing cycles. Unfortunately the reinforcement used is UD so the results are not directly comparable. As UD-laminates have more fibre in the bending direction of the test higher test values are expected. The results found in Figure 10.1a is therefore reasonably high. This support the clam that this is a good laminate in flexural strength.

10.2 Surface finish and void content

T1 was moulded with proper debulking but no resin injection. The bad surface finish obtained originated hypothetically from enclosed air during preform placing and tool closing. Consequently T2 was moulded with vacuum closing of the tool. Test T2 resulted in only a minor improvement of the surface finish. Therefore vacuum closing of the tool was abandoned as a malfunctioning solution. It is suggested as an implication of this result that the air apparently inhabiting the surface of T1 an T2 does not come from enclosed air, but arise from elsewhere. As a matter of fact this "air" might not be air at all. It appears as air bubbles but it

might arise from other gases or particles. It is well known that prepreg contains volatiles that evaporate upon curing if their vapor pressure is higher than the resin pressure. As no measures were taken in order to elevate the resin pressure in T1 and T2 it is found likely that the bubbles on the surface persist due to precipitated volatiles in the prepreg. As the resin pressure is elevated and kept hydrostatic these bubbles vanish. This is accomplished in tests T3 and T4. In addition to bubbles there were white dots on the surface of both T2 and T1. The latter more severely than the first. In earlier work [27] the author talked about this as ambiguous surface flaws which were not fully understood. However, when the mould release system was changed[2] before moulding test Tc1 these white dots disappeared. They are consequently interpreted as residuals from the release agent and therefore not discussed any further in this text. In both test T3 and T4 high quality surface finish was obtained. Besides good surface finish T3 and T4 also yield lower void content than the other tests. T1 and T2 show some of intralaminar voids. Such voids are not observed in T3 and T4 which are virtually void free. As no other tests were able to obtain void free laminates with good surface finish and resin injection is the functionality that distinguishes T3 and T4 from T1 and T2 the inference that resin injection provides both surface finish and low void content for the laminate is quickly suggested. The objective of the resin injection is to elevate the resin pressure. As different sources conclude [10, 15], and the aforementioned experiments indicate – high resin pressure is necessary to produce high quality laminates[3] with good surface finish and low void content.

[2]The mould release was changed from Chemlease® 880 to Frekote 44-NC™
[3]This is at least true for prepreg systems intended for autoclave curing.

Chapter 11

Conclusion

The process of moulding prepreg in closed moulds with resin injection, called SQRTM was tested and investigated. The main concern of this work was to better understand the governing process mechanisms in the SQRTM method and to achieve high quality laminates. Process parameters were mainly evaluated with respect to void content, surface quality and interlaminar shear strength. The process parameters were pressure, temperature, debulking, viscosity and similarity of injection resin and prepreg resin. The scope of the work was limited to simple geometries and the available materials. Several laminates were moulded with and without resin injection and preform debulking. The laminates obtained were tested with short beam shear tests and visually inspected by microscopic and photographic techniques.. The investigation indicated that a high quality surface finish is accomplished when elevated hydrostatic resin pressure is obtained in the mould cavity. It is suggested, both from experiments and CFD analyses, that a thorough understanding of the resin rheology should be appreciated by the designer of the process. Mainly the viscosity of the injected resin should be low. It was not necessary to use separate surface plies to obtain a good surface finish, but a good appropriate mould release system should be used. Furthermore, it is suggested that debulking of the prepreg preform yields higher flexural strength. By exploring the laminates

with microscopes it was found that a combination of preform debulking and elevated resin pressure yields nearly void free laminates. Some tests were performed where the prepreg resin and injection resin had very different curing characteristics. The resulting laminates were of poor quality, showing that matched properties are important.

SQRTM offers a new production method for high performance composites. The process removes the need for expensive autoclaves and it makes machining after cure unnecessary. This work has shown that high quality laminates can be made if production parameters are properly controlled.

Chapter 12

Further work

This thesis has investigated the possibilities for making good laminates with the SQRTM technique. For further enhancement of the system the following are proposed by the author:

Versatility: In order to make the process as lean as possible lower bounds for the process parameters have to be established. How little debulk and how little resin pressure that is viable for the process will be interesting.

Data acquisition: The process parameters can be monitored through sensors implemented in the mould tool. Pressure sensors were bought during this work but delay in delivery made implementation impossible. Future student might implement these in the tool. Further, the CFD analyses can be validated with pressure sensors.

Bibliography

[1] T. Kruckenberg and R. Paton, editors. *Resin Transfere Moulding for Aerospace Structures*. Kluwer Academic Publishers, 1998.

[2] K. D. Potter. The early history of the resin transfer moulding process for aerospace appications. *Composites Part A: applied science and manufacturing*, 30:619–621, 1999.

[3] Doh Hoon Lee, Woo Il Lee, and Moon Koo Kang. Analysis and minimization of void formation during resin transfer molding process. *Composite Science and Technology*, 66:3281–3289, 2006.

[4] Simon Bickerton et al. Design and application of actively controlled injection schemes for resin-transfer molding. *Composite Science and Technology*, 61: 1625–1637, 2001.

[5] Constantin Chassapis Vojin Jovanovic, Souran Manoocheheri. Parameter estimation for resin transfer molding. *Engineering Computations*, Vol. 18(8): 1091–1107, 2001.

[6] S. Black. Sqrtm enables net-shape parts: Composites world. *High-Performance Composites*, 18(5), 2010. URL www.scopus.com.

[7] Hexcel. *Technical data sheet: HexPly® 6376C-905-36%*, 2005.

[8] *Technical data sheet: UMECO LTM®10, LTM®12 and LTM®16 TOOLING PREPREGS*. Umeco structural materials, 2012.

[9] A. R. Upadhya, G. N. Dayananda, G. M. Kamalakannan, J. Ramaswamy Setty, and J. Christopher Daniel. Autoclaves for aerospace applications: Issues and challenges. *International Journal of Aerospace Engineering*, 2011.

[10] F. C. Campbell. Manufacturing processes for advanced composites. URL http://www.knovel.com/web/portal/browse/display?_EXT_KNOVEL_DISPLAY_bookid=4377.

[11] Abaqus manual, 2012. URL http://ivt-abaqusdoc.ivt.ntnu.no:2080/v6.12/index.html.

[12] R. Byrond Bird, Warren E. Stewart, and Edwind N. Lightfoot. *Transport Phenomena*. John Wiley and Sons, Inc., 2nd edition, 2002.

[13] LászlóP. Kollár and George S. Springer. Mechanics of composite structures. URL http://www.knovel.com/web/portal/browse/display?_EXT_KNOVEL_DISPLAY_bookid=2329.

[14] N.P. Vedvik. Essential mechanics of composites. Internal NTNU document, 2012.

[15] P. Olivier, J.P. Cottu, and B. Ferret. Effects of cure cycle pressure and voids on some mechanical properties of carbon/epoxy laminates. *Composites*, 26(7):509 – 515, 1995. ISSN 0010-4361. doi: 10.1016/0010-4361(95)96808-J. URL http://www.sciencedirect.com/science/article/pii/001043619596808J.

[16] Michael R. Wisnom. Modelling the effect of cracks on interlaminar shear strength. *Composites part A*, 1996.

[17] L.W. Davies, R.J. Dayand D. Bond, A. Nesbitt, and E. Gardon J. Ellis. *Effect of cure cycle heat transfer rates on the physical and mechanical properties of an epoxy matrix composite*. Composite Science and technology, 2007.

[18] Standard test method for short-beam strength of polymer matrix composite materials and their laminates1. Standard D2344/D2344M, *American Society for Testing and Materials* (ASTM), 2006.

[19] Frank M. White. *Fluid Mechanics*. MCGaw Hill, 2008.

[20] A. G. Straatman Betchen, L. and B. E. Thompson. A nonequilibrium finite-volume model for conjugate fluid/porous/solid domains. *Numerical Heat Transfer, Part A*, 49:543–565, 2006.

[21] T. Centea and P. Hubert. Modelling the effect of material properties and process paramerters on tow impregnation in out-of-autoclave prepregs. *Composites Part A: applied science and manufacturing*, 43:1505–1513, 2012.

[22] *Technical data sheet: HexPly® M56*. Hexcel, March 2010.

[23] Tor Sigurd Breivik. Email correspondation with Tor Sigur Breivik at kda. Email, February 2013.

[24] D H-J A Lukaszewicz and K Potter. Through-thickness compression response of uncured prepreg during manufacture by automated layup. *Proceedings of the Institution of Mechanical Engineers Part B: Journal of Engineering Manufacture*, 2012.

[25] Radius engineering. An overview of radius' rtm / sqrtm injection equipment offerings. PDF.

[26] *O-ringer som tetningselement*. Otto Olsen AS, 2012.

[27] Simen Johnsen. Closed form net shape processing og composites. Project work, NTNU, December 2012.

[28] JCH Technologies. URL http://www.rtmcomposites.com/equipment/rtm-lrtm-injection/infuser-prg.

[29] German Lloyd. *Technical data sheet: EPIKOTE Resin MGS® RIMR 135 and EPIKOTE Resin MGS® RIMR 135 and EPIKURETM Curing Agent MGS® RIMH 134–RIMH 137*. Momentive, August 2006.

[30] *ABAQUS manual: Getting Started with Abaqus: Keywords Edition*, chapter 4.1 Element formulation and integration. Simulia.

[31] *Technical data sheet: HexPly 6376.* Hexcel, March 2007.

[32] Fridtjov Irgens. *Formelsamling mekanikk.* Tapir akademiske forlag, 1999.

Appendix A

Matlab Scripts

Laminate Stiffness Matrix:

```
%This script calculates the ABD-matrix for a given laminate
%ply
E1=67000;%MPa
E2=67000;%MPa
G12=7000;%MPaG12=45000;%MPa
v12=0.27;


%%%%%%%%%%
v21=(E2/E1)*v12;
Q11=E1/(1-v12*v21);
Q12=v12*E2/(1-v12*v21);
Q22=E2/(1-v12*v21);
Q66=G12;
Q=[Q11,Q12,0;Q12,Q22,0;0,0,Q66];

n=8;%antall lag

t=0.268;%tykkelse mm/lag
Vinkel=[0 90 0 90 0 90 0 90];%vinklene angis

```

```
22
23 QQQ=zeros(3,3*n); %Transformert stivhetsmatrise for alle lagene
24 for j=1:n
25     s=sind(Vinkel(j));
26     c=cosd(Vinkel(j));
27     %t1=Vinkel(j);
28 %T=[cosd(t1) -sind(t1) 0; sind(t1) cosd(t1) 0;0 0 1];
29 Qn(1,1)=Q11*c^4+2*(Q12+2*Q66)*c^2*s^2+Q22*s^4;%inv(T)*Q*(T);
30 Qn(1,2)=(Q11+Q22-4*Q66)*c^2*s^2+Q12*(c^4+s^4);
31 Qn(2,2)=Q11*s^4+2*(Q12+2*Q66)*c^2*s^2+Q22*c^4;
32 Qn(1,3)=(Q11-Q12-2*Q66)*c^3*s+(Q12-Q22+2*Q66)*c*s^3;
33 Qn(2,3)=(Q11-Q12-2*Q66)*s^3*c+(Q12-Q22+2*Q66)*s*c^3;
34 Qn(3,3)=(Q11+Q22-2*Q12-2*Q66)*c^2*s^2+Q66*(c^4+s^4);
35 Qn(2,1)=Qn(1,2);
36 Qn(3,2)=Qn(2,3);
37 Qn(3,1)=Qn(1,3);
38
39 for k=1:3
40     for l=1:3
41         QQQ(k,(3*j+l)-3)=Qn(k,l);
42     end
43 end
44 end
45
46 HA=t;
47 A=zeros(3);
48 B=zeros(3);
49 D=zeros(3);
50 for ii=1:n
51     H(ii)=(ii*t-t)-n*t/2; %angir lagkoordinater
52 end
53 H(n+1)=(n*t)-n*t/2;
54
55 for p=1:n %Summerer A,B og D
56 for m=1:3
57     for o=1:3
58         A(m,o)=A(m,o)+QQQ(m,o+3*p-3)*(H(p+1)-H(p));
59         B(m,o)=B(m,o)+0.5*QQQ(m,o+3*p-3)*(H(p+1)^2-H(p)^2);
60         D(m,o)=D(m,o)+(1/3)*QQQ(m,o+3*p-3)*(H(p+1)^3-H(p)^3);
```

```
    end
end
end

LSM=zeros(6); %Setter sammen ABD matrisen
for u=1:3
    for v=1:3
        LSM(u,v)=A(u,v);
        LSM(u+3,v)=B(u,v);
        LSM(u,v+3)=B(u,v);
        LSM(u+3,v+3)=D(u,v);
    end
end

ABD=LSM;
disp(LSM)
```

Viscosity – Flow length plot:

```
%Time ? Length of flow  plot

K=3e-11; %3e-11m^2, Permeability
DP=-1e5;%Pa, Delta pressure
mu=[10000,1000,100,10,5.5];%Pa.s, The different viscosities
L=[0.00:0.0001:0.01];%m, The lengthscale of the flow

%Plot aestetic values

m=['\mu = 10000 Pa s';'\mu = 1000 Pa s ';'\mu = 100 Pa s  ';...
    '\mu = 10 Pa s   ';'\mu = 5.5 Pa s  '];%Legend
st=['-';'-';'-';'-';'-']; %Line styles
c=['r';'b';'g';'y';'k']; %Line color

%CALCULATIONS

% v=(K/mu) DP  %== Darcy's Law
% (v=(K/mu) DP)|/L  %Deviding by Length gives:
% 1/t=K/mu DP/(L^2) %Inverse time scale

```

```
21 %THE ABOVE RESULT IS PLOTED FOR DIFFERENT VALUES AS FOLLOWS:
22
23 for i=1:5
24
25     revtime=-(K*DP./(mu(i).*(L.^2))); %Inverse time
26     t=1./(60*revtime);%minutes
27     semilogy(L,t,c(i),'LineStyle',st(i),'LineWidth',1.5) ...
       %Plot with logaritmic y-axis
28
29      hold on
30 end
31 ylabel('Time [minutes]','FontSize',20)
32 xlabel('Length of flow [m]','FontSize',20)
33
34 Leg=legend(m,'Location','SouthEast');
35 set(Leg,'Fontsize',15);
36
37 set(gcf, 'PaperPositionMode', 'auto');
38
39
40 filename='airvac.eps';
41 print( '-depsc2', filename) %Prints the plot fileshowed in ...
       the thesis
42 fixPSlinestyle(filename)
```

Appendix B

Three point bend test – Results and calculations

Shear stress vs. normal stress

The ratio between maximum shear stress ($\tau_{\max}$) and maximum normal stress ($\sigma_{\max}$) in a three point bending specimen is computed according to Figure B.1. The maximum shear stress occur at the neutral line of the specimen and the maximum normal stress arises at the extremes of the center line. The maximum tension point is indicated.

Wisnom [16] states that:

$$\tau_{\max} = 0.75 \cdot \frac{F}{D \cdot B} \tag{B.1}$$

From Irgens [32] we know that:

$$M_{\max} = \frac{1}{4} F \cdot L \tag{B.2}$$

$$\sigma_{\max} = \frac{M_{\max}}{I} \cdot y_{\max} \tag{B.3}$$

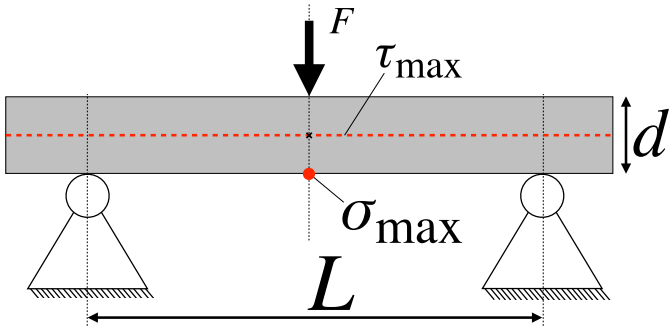

FIGURE B.1: Illustration of the three point bending beam. The plane of maximum shear and point of maximum normal stress is indicated. The beam has a out of plane depth, B.

Which implies that:

$$\sigma_{\max} = \frac{3}{2}\frac{FL}{D^2 B} \tag{B.4}$$

By divison the following relationship between shear stress and normal stress is obtained:

$$\frac{\tau_{\max}}{\sigma_{\max}} = \frac{1}{2}\frac{D}{L} \tag{B.5}$$

Short beam shear plots

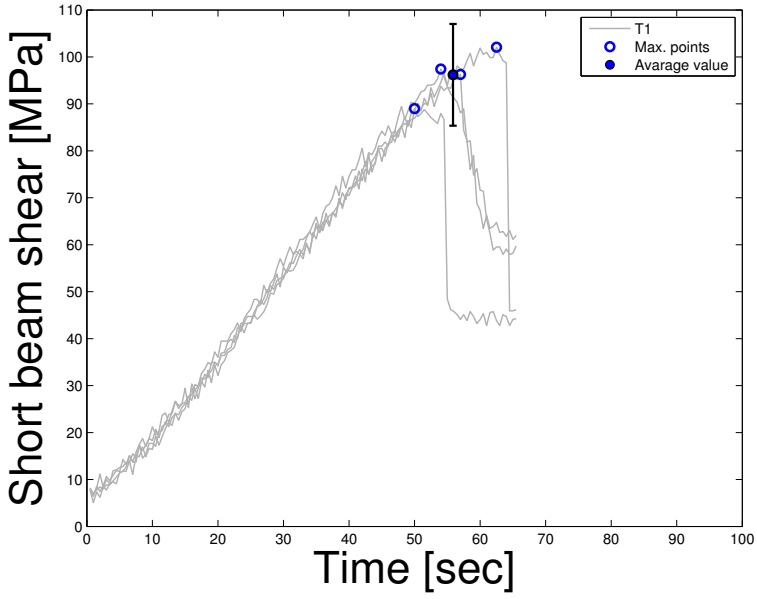

(A)

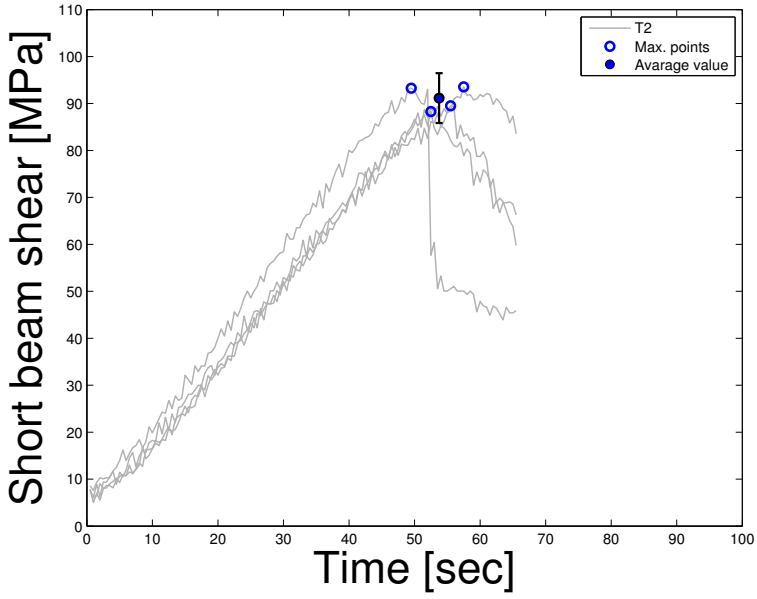

(B)

FIGURE B.2: The Figure shows Force – Time plot for the different samples from test T1 and T2. The average error bar is ±2 standard deviations.

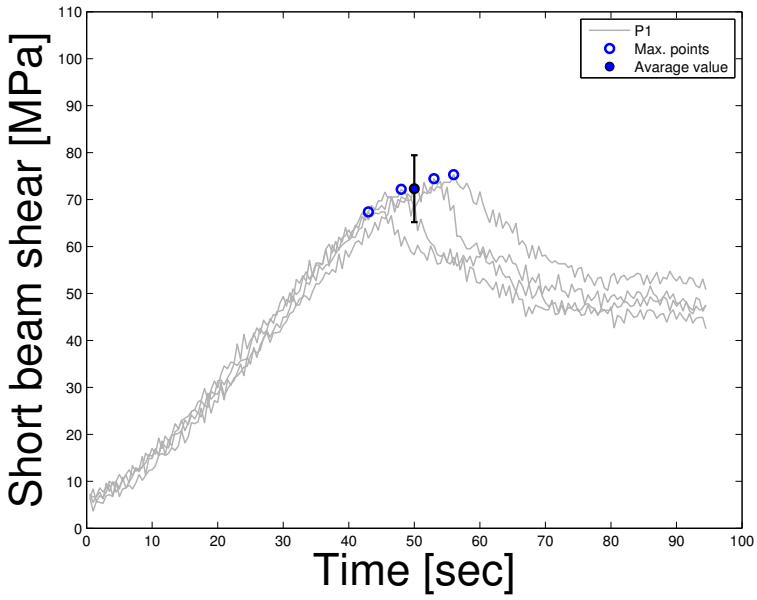

(A)

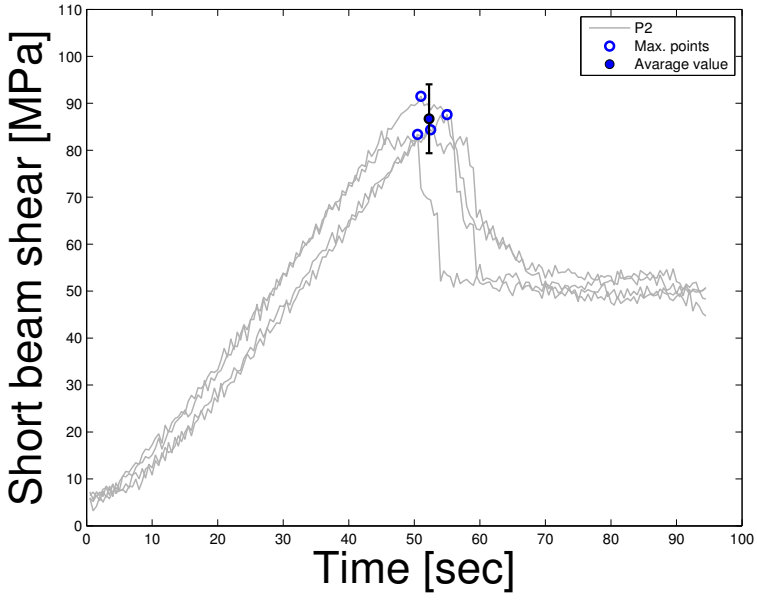

(B)

FIGURE B.3: The Figure shows Force – Time plot for the different samples from test P1 and P5. The average error bar is ±2 standard deviations.

Appendix C

Thermal expansion calcultation

Stresses and strains due to thermal expansion of the tool in calculated in this appendix.

After the first moulding in the project a displacement of 0.78 mm was measured.

$$\epsilon = \frac{0.78\,\text{mm}}{260\,\text{mm}} = 0.003 \tag{C.1}$$

By applying the engineering constants from the three point bending simulation in the Laminate Stiffness Matrix script in Appendix A the following calculations were done:

$$\begin{Bmatrix} N_x \\ N_y \\ N_{xy} \\ M_x \\ M_y \\ M_{xy} \end{Bmatrix} = \left[\begin{array}{ccc:ccc} 1.5\cdot10^5 & 0.1\cdot10^5 & 0 & 0 & 0 & 0 \\ 0.1\cdot10^5 & 1.5\cdot10^5 & 0 & 0 & 0 & 0 \\ 0 & 0 & 0.6\cdot10^5 & 0 & 0 & 0 \\ \hdashline 0 & 0 & 0 & 0.6\cdot10^5 & 0.04\cdot10^5 & 0 \\ 0 & 0 & 0 & 0.04\cdot10^5 & 0.6\cdot10^5 & 0 \\ 0 & 0 & 0 & 0 & 0 & 0.2\cdot10^5 \end{array}\right] \begin{Bmatrix} 0.003 \\ 0.003 \\ 0 \\ 0 \\ 0 \\ 0 \end{Bmatrix} \tag{C.2}$$

This gives the following forces from the laminate:

$$\begin{Bmatrix} N_x \\ N_y \\ N_{xy} \\ M_x \\ M_y \\ M_{xy} \end{Bmatrix} = \begin{Bmatrix} 468.42 \\ 468.42 \\ 0 \\ 0 \\ 0 \\ 0 \end{Bmatrix} \tag{C.3}$$

Accordingly the maximum shear stress in the mould flange are calculated:

$$\tau_{max} = \frac{3}{2}\frac{V}{A} = \frac{3}{2}\frac{468.4\,\mathrm{N\,mm^{-1}}}{10\,\mathrm{mm}} = \underline{\underline{70.3\,\mathrm{MPa}}} \tag{C.4}$$

For the laminate ply stress the matlab script gives the local stiffness matrix:

$$\begin{Bmatrix} \sigma_1 \\ \sigma_2 \\ \tau_{12} \end{Bmatrix} = \begin{bmatrix} Q_{11} & Q_{12} & Q_{16} \\ Q_{12} & Q_{22} & Q_{26} \\ Q_{16} & Q_{26} & Q_{66} \end{bmatrix} \begin{Bmatrix} \epsilon_1 \\ \epsilon_2 \\ \gamma_{12} \end{Bmatrix} = \begin{bmatrix} 6.7\cdot10^4 & 0.5\cdot10^4 & 0 \\ 0.5\cdot10^4 & 6.7\cdot10^4 & 0 \\ 0 & 0 & 2.8\cdot10^4 \end{bmatrix} \begin{Bmatrix} 0.003 \\ 0.003 \\ 0 \end{Bmatrix} \tag{C.5}$$

The laminate stress is thus,

$$\sigma_1 = \sigma_2 = \underline{\underline{218.5\,\mathrm{MPa}}} \tag{C.6}$$

None of these values are dangerously high.

Appendix D

Results from earlier work

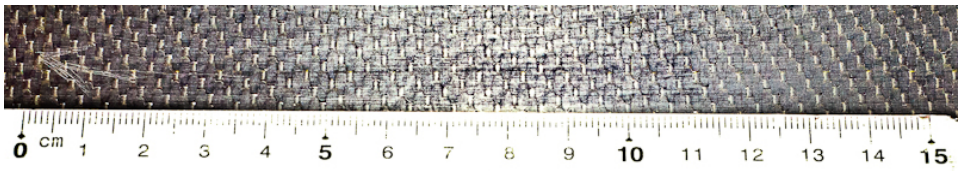

(A) P1

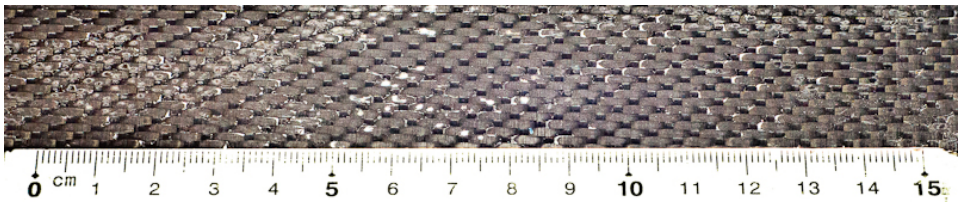

(B) P5

FIGURE D.1: The surface on test P1 and P5 depicted. White dots and surface flaws can be seen.

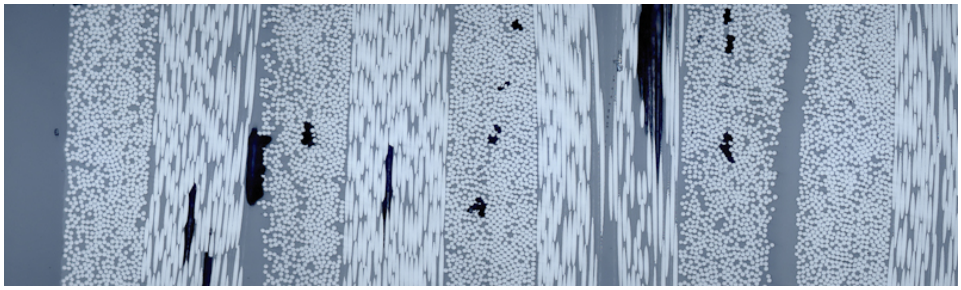

(A) P1

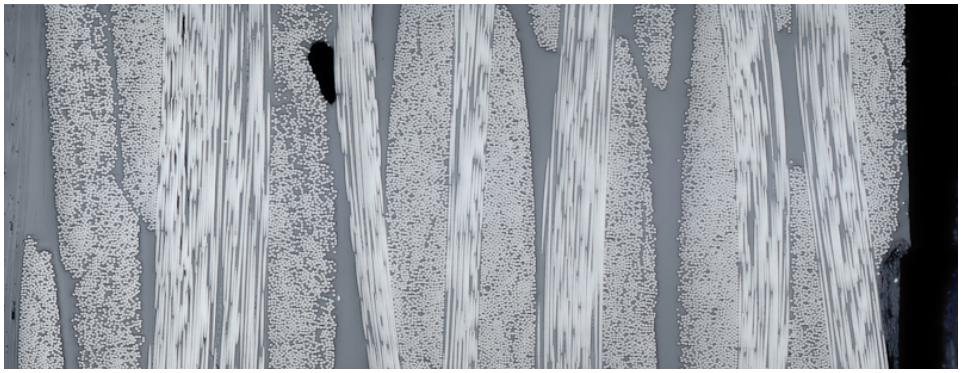

(B) P5

FIGURE D.2: Microscopy pictures of the internal structure in P1 and P5. A distinct improvement from P1 to P5 is shown.

TABLE D.1: Tabular representation of the experiments included from the project.

Test	External resin pressure	Dwell at 175 °C [min]	Applied vacuum	Debulk	Layup	Material
P1	N/A	83	N/A	N/A	8 plies	A
P5	7 bar	120	Yes	5 hours on entire stack	8 plies	A

Appendix E

Machine drawings

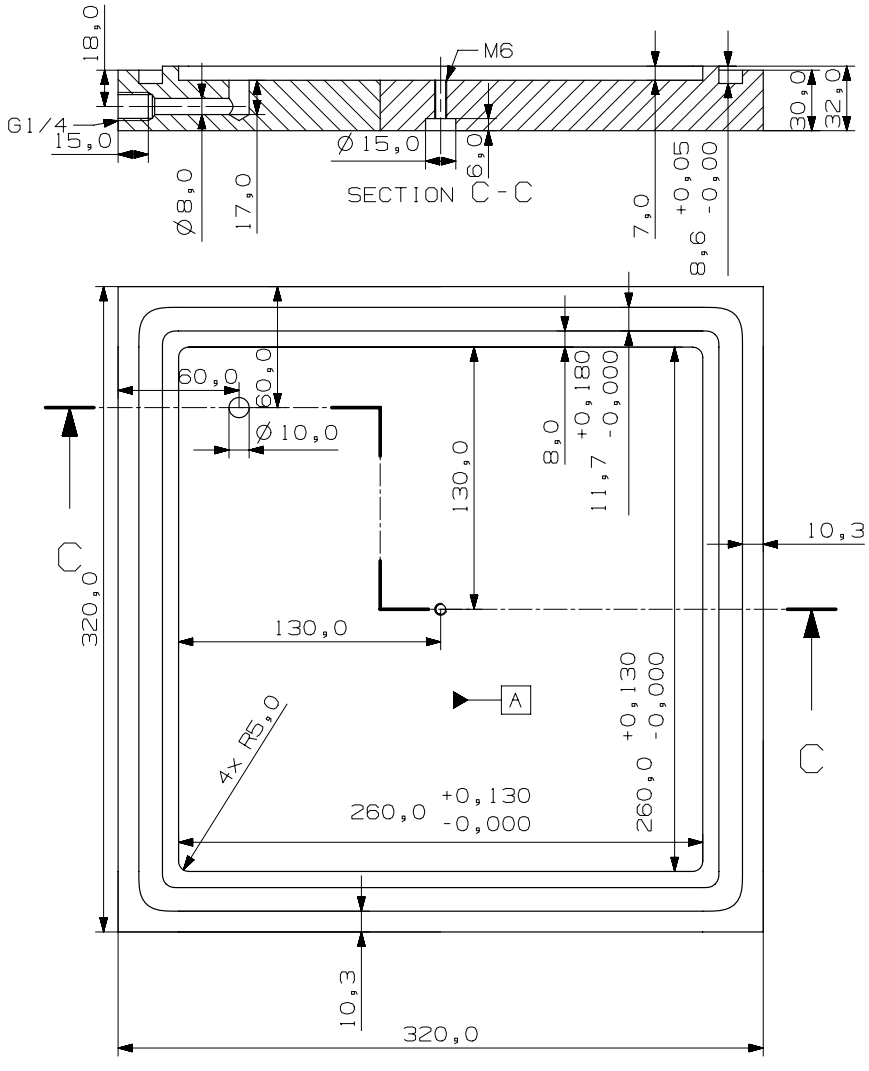

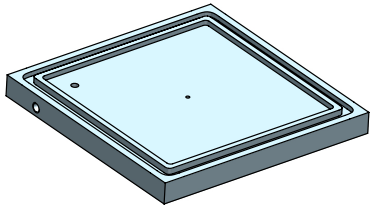

Flate A poleres etter avtale

▱	0.05	A

Dato	Konstr./Tegnet	Godkjent	Maalestokk	NTNU - IPM
16.10.12	Simen Johnsen	Projeksjonsmetode	1:2	
Hunform			Erstatning for:	Erstattet av:
Henvisning:	Beregning:		Materiale: Alumec	

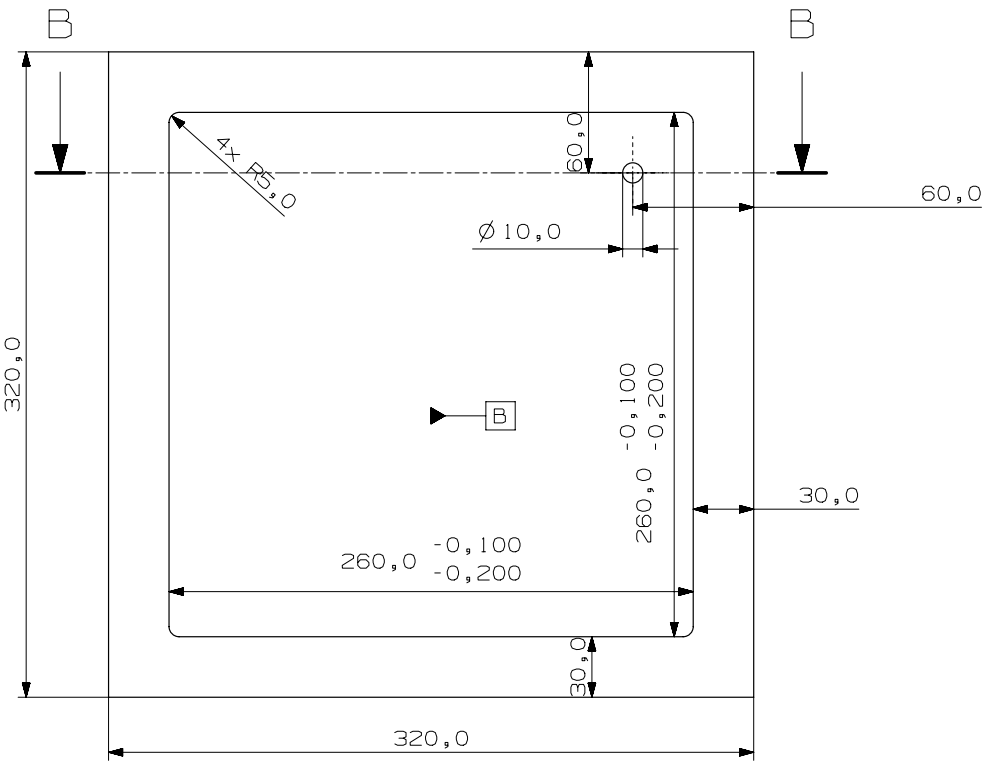

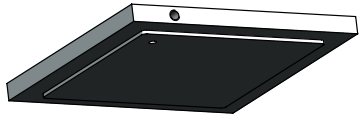

Flate B poleres etter avtale

0.05 B

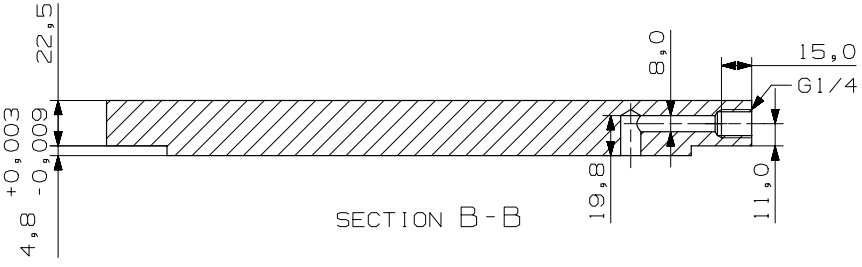

Dato: 16.10.12	Konstr./Tegnet: Simen Johnsen	Godkjent: Projeksjonsmetode	Maalestokk: 1:2	NTNU - IPM
Hanform			Erstatning for:	Erstattet av:
Henvisning:	Beregning:		Materiale: Alumec	

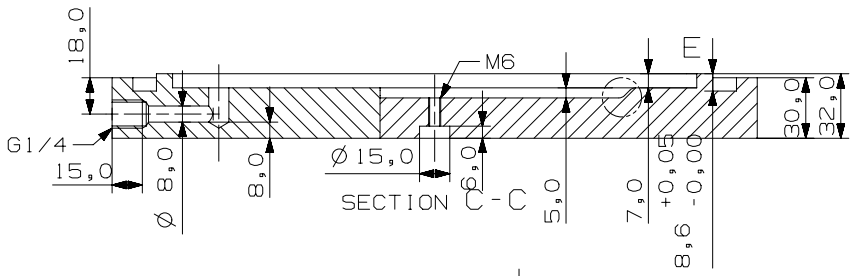

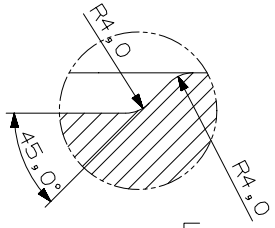

DETAIL E
SCALE 2:1

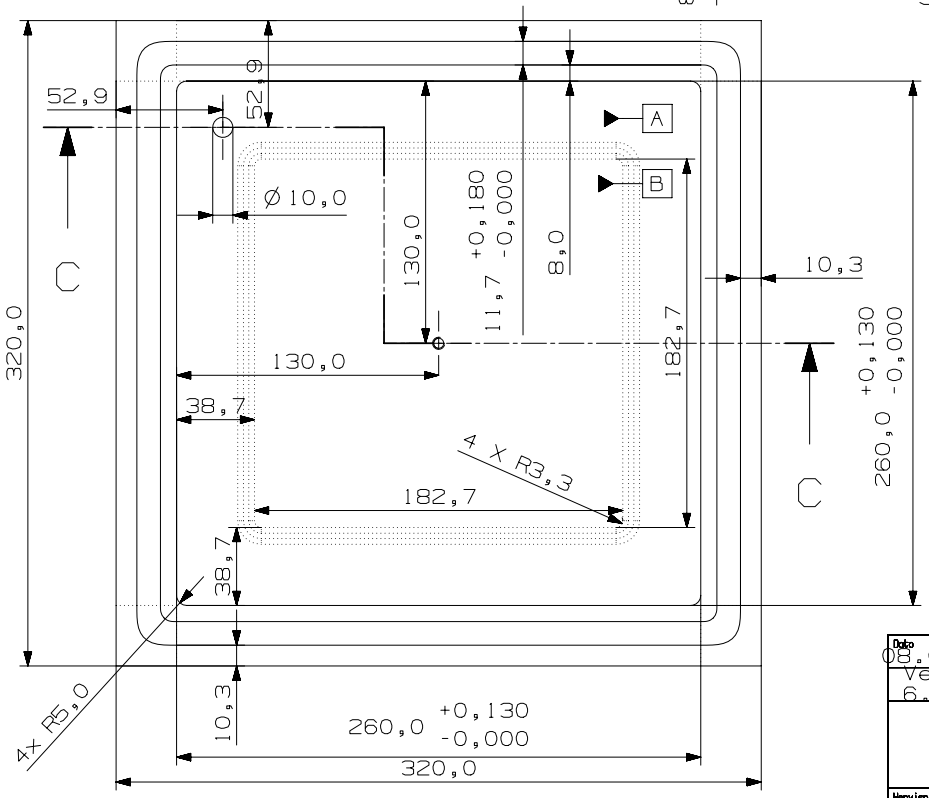

Flate A og B, samt overgang mellom, poleres etter avtale.

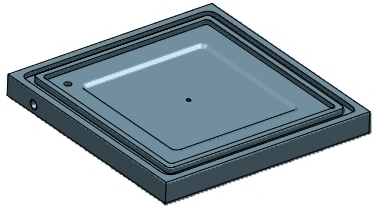

Dato: 08.03.13	Konstr./Tegnet: Simen Johnsen	Godkjent:	Maalestokk: 1:2	NTNU - IPM
Vekt: 6.7kg		Prosjektnummer:		
Hunform m. utsparing			Erstatning for:	Erstattet av:
Henvisning:		Beregning:	Materiale: AA 6061	

Appendix F

HSE form

Sikkerhets- og kvalitetsgjennomgang av laboratorietester og verkstedsarbeid

Safety and Quality Evaluation of Activities in the Laboratory and Workshop

Perleporten

1 Identifikasjon - *Identification*	**Dokumentnr. – *Document no.*:**	
Kundenavn – *Customer name* **Simen Johnsen**	Prosjektnavn – *Project name* **SQRTM net shape processing of composites**	Projektnr. – *Project no.* **69450723**
Beskrivelse av arbeid – *Description of job* **Closed mould processing with hot vacuum debulking and resin injection**		Dato – *Date* **15.04.13 – 10.06.13**

2 Projekt - *Team*			
Prosjektleder og organisasjon – *Project manager and organization*	**Simen Johnsen NTNU**	Ansvarlig for instrumentering – *Responsible for instrumentation.*	**Simen Johnsen**
Leiestedsansvarlig – *Laboratory responsible*	**Jon Harald Grave**	Operatør – *Operator*	**Simen Johnsen**
Auditør for sikkerhets og kvalitetsgjennomgang – *Auditer for safety check*	**Andreas Echtermeyer**	Ansvarlig for styring av forsøk – *Responsible for running the experiment.*	**Simen Johnsen**
Ansvarlig for eksperimentelt faglig innhold – *Responsible for experimental and scientific content*	**Simen Johnsen**	Ansvarlig for logging av forsøksdata – *Responsible for logging and storing experimental data*	**Simen Johnsen**
Ansvarlig for dimensjonering av last og trykkpåkjente komponenter – *Reponsible for dimensioning load bearing and pressurized components*	**Simen Johnsen**	Ansvarlig for montering av testrigg – *Responsible for building the rig*	–

3 Viktig!! – *Important!!*	J: Ja – *Yes* / N: Nei - *No*
Er arbeidsordren signert? – *Is the work order signed?*	**Yes**
Trenger operatøren kurs i bruk av maskinen(e)? – *Does the operator need training on the equipment?*	**Yes**
Har operatøren sikkerhetskurs? (påbudt) – *Has the operator followed the safety courses? (mandatory)*	**Yes**

4.1 Sikkerhet – *Safety* (Testen medfører – *The test contains*)	J: Ja – *Yes* / N: Nei - *No*		
Stor last – *Big loads*	**Yes**	Brannfare – *Danger of fire*	**No**
Tunge løft – *Heavy lifting*	**No**	Arbeid i høyden – *Working at heights*	**No**
Hengende last – *Hanging load*	**No**	Hydraulisk trykk – *Hydraulic pressure*	**No**
Gasstrykk – *Gas pressure*	**No**	Vanntrykk – *Water pressure*	**No**
Høy temperatur – *High temperature*	**No**	Lav temperatur – *Low temperature*	**No**
Deler i høy hastighet – *Parts at high velocity*	**No**	**Farlige kjemikalier – *Dangerous chemicals***	**Yes**
Sprutakselerasjon ved brudd – *Sudden acceleration at fracture/failure*	**No**	Forspente komponenter – *Pre-tensioned components*	**Yes**
Farlig støv – *Dangerous dust*	**No**	Kraftig støy – *Severe noise*	**No**
Klemfare – *Danger of pinching*	**Yes**	Roterende deler – *Rotating parts*	**No**

4.2 Påkrevet verneustyr – *Required safety equipment*	J: Ja – *Yes* / N: Nei - *No*		
Briller (påbudt) – *Glasses (mandatory)*	**Yes**	Vernesko – *Safet shoes*	**No**
Hjelm – *Helmet*	**No**	**Hansker – *Gloves***	**Yes**
Skjerm – *Screen*	**Yes**	Visir – *Visir*	**No**

Hørselsvern – *Earprotection*	No	Løfteredskap – *Lifting equipment*	No
Yrkessele, fallsele, etc. – *Harness ropes, other measures to prevent falling down.*	No		

Sikkerhets- og kvalitetsgjennomgang av laboratorietester og verkstedsarbeid

NTNU
Perleporten

5.1 Beskrivelse av aktivitet – *Description of the activity (see Appendix)*

Vurdering skal være basert på en skriftlig prosedyre for bruk av maskinen. I enkelte tilfeller kan prosedyre bli beskrevet direkte i tabellen nedenfor.

The evaluation shall be based on a written operating procedure for the machine. For simple cases the procedure can be directly described in the tables below.

Nr.	Beskrivelse av aktivitet – *Description of activity*	Fare - *Danger*	Prosedyre nr. – *Procedure no.*	Sannsynlighet – *Probability*	Konsekvens – *Consequence*	Risiko – *Risk*
1	**Closed mould processing in hot press**	Resin/hardener evaporations intoxication	1	1	3	3
		Burn by Hotpress or heated mould	2	4	1	4
2	**Hot vacumm debulking**	Burn by oven	3	3	1	3
3	**Resin Injection**	Burst in pressurized resin tubes	4	1	3	3

5.2 Korrigerende Tiltak – *Corrective Actions*

Nr.	Korrigerende tiltak – *Corrective action*	Sannsynlighet – *Probability*	Konsekvens – *Consequence*	Risiko – *Risk*	Utført dato – *Date of action*
1	Good ventilation of curing area	1	2	2	15.04.13
2	Use gloves and be carful with the heated objects + use glass door	2	1	2	15.04.13
3	Use gloves and be carful with the heated objects	2	1	2	15.04.13
4	Use plastic screen	1	1	1	15.04.13

Sikkerhets og kvalitetsgjennomgang av laboratorietester og verkstedsarbeid

NTNU
Perleporten

5.3 Feilkilder – *Reasons for mistakes/errors*

Sjekkliste: Er følgende feilkilder vurdert? – Check list: Is the following considered? J: Ja – *Yes* / N: Nei - *No*

Tap av strøm – *Loss of electricity*	No	Overspenning – *Voltage surge*	No
Elektromagnetisk støy – *Electromagnetic noise*	No	Manglende aggregatkapasitet av hydraulikk – *Insufficient power of the machine*	No
Jordfeil – *Electrical earth failure*	No	Vannspurt – *Water jet*	No
Ustabilt trykk av hydraulikk/kraft – *Unstable pressure or hydraulic force*	No	Tilfeldig avbrudd av hydraulikk/kraft – *Unintended interruption of power supply*	No
Last-/ forskyvnings grenser etablert? – *Are load and displacement limits established?*	No	Lekkasjer (slanger/koblinger, etc.) – *Leakage of pipes, hoses, joints, etc.*	No
Mulige påvirkninger fra andre aktiviteter – *Possible interference from other activities*	Yes	Mulige påvirkninger på andre aktiviteter – *Possible interference towards other activities*	Yes
Problemer med datalogging og lagring – *Troubles in loading and storage*	No	Brann i laboratoriet – *Fire in the laboratory*	No

6 Kalibreringsstatus for utstyr – *Calibration of equipment*

(ex: load cell, extensometer, pressure transducer, etc)

I.D.	Utstyr - *Equipment*	Gyldig til (dato) – *Valid until (date)*

7 Sporbarhet – *Traceability*

Eksisterer – *Is there* J: Ja – *Yes* / N: Nei - *No*

Er alle prøvematerialene kjente og identifiserbare? – *Are all experimental materials known and traceable?*	Yes
Eksisterer det en plan for markering av alle prøvene? – *Is there a plan for marking all specimens?*	Yes
Er dataloggingsutstyret identifisert? – *Is the data aquisition equipment identified?*	-
Er originaldata lagret uten modifikasjon? – *Is the original data stored safely without modification?*	-
Eksisterer det en backup-prosedyre? – *Is there a back-up procedure for the data (hard disk crash)?*	-
Eksisterer det en plan for lagring av prøvestykker etter testing? – *Is there a plan for storing samples after testing?*	-
Eksisterer en plan for avhending av gamle prøvestykker? – *Is there a plan for disposing of old samples?*	Yes

8 Kommentarer – *Comments*

9 Signaturer – *Signatures*

Godkjent (dato/sign) – Approved (date/signature)

Prosjektleder – *Project leader*	Verifikatør – *Verifier*	Godkjent – *Approved by*